Seasonal and Intraseasonal Variability of Mesoscale Convective Systems over the South Asian Monsoon Region

Katrina S. Virts[1] and Robert A. Houze, Jr.[1,2]

[1]Department of Atmospheric Sciences, University of Washington, Seattle, Washington

[2]Pacific Northwest National Laboratory, Richland, Washington

Submitted to the *Journal of the Atmospheric Sciences*, 11 January 2016

Revised: 24 May 2016

Corresponding author address: Dr. Katrina Virts, Current affiliation: Department of Atmospheric Science, University of Alabama in Huntsville, 320 Sparkman Dr., Huntsville, AL 35805

Email: katrina.virts@nsstc.uah.edu

Abstract

Seasonal and intraseasonal differences in mesoscale convective systems (MCSs) over South Asia are examined using A-Train satellites, a ground-based lightning network, and reanalysis fields. Pre-monsoon (April-May) MCSs occur primarily over Bangladesh and the eastern Bay of Bengal. During the monsoon (June-September), small MCSs occur over the Meghalaya Plateau and northeast Himalayan notch, while large and connected MCSs are most widespread over the Bay of Bengal. Monsoon MCSs produce less lightning and exhibit more extensive stratiform and anvil reflectivity structures in CloudSat observations than do pre-monsoon MCSs.

During the monsoon season, Bay of Bengal and Meghalaya Plateau MCSs vary with the 30-60 day northward-propagating intraseasonal oscillation, while northeast Himalayan notch MCSs are associated with weak large-scale anomalies but locally enhanced CAPE. During intraseasonal active periods, a zone of enhanced large and connected MCSs, precipitation, and lightning extends from the northeastern Arabian Sea southeast over India and the Bay of Bengal, flanked by suppressed anomalies. Spatial variability is observed within this enhancement zone: lightning is most enhanced where MCSs are less enhanced, and vice versa. Reanalysis composites indicate that Bay of Bengal MCSs are associated with monsoon depressions, which are frequent during active monsoon periods, while Meghalaya Plateau MCSs are most frequent at the end of break periods, as anomalous southwesterly winds strengthen moist advection toward the terrain. Over both regions, MCSs exhibit more extensive stratiform and anvil regions and less lightning when the large-scale environment is moister, and vice versa.

1. Introduction

The annual cycle over southern Asia (Fig. 1) is dominated by seasonally varying monsoon circulations (Webster et al. 1998). The summer monsoon [during June-September (JJAS); hereafter, the monsoon] is associated with a low-level trough over northern India and a northward shift of the tropical convergence zone in this sector (Fig. 2b; Webster et al. 1977). Southwesterly winds advect moisture from the Indian Ocean over the landmass, producing frequent rainfall over much of South Asia. Precipitation maxima are observed at or just upstream of where the low-level moist flow encounters steep terrain (Fig. 2b; the seasonal cycle is discussed in more detail in Section 3).

Earlier observations including those during the Monsoon Experiment (MONEX, 1978-79) indicated that monsoon precipitation is not primarily associated with isolated deep convective towers but rather with mesoscale rain areas with embedded deep convection (Ramage 1971; Houze and Churchill 1987), categorized as mesoscale convective systems (MCSs; Houze 2014, Chapter 9). Recent work has examined the geographic distribution of various types of precipitating systems during the monsoon using observations from the Tropical Rainfall Measuring Mission (TRMM) satellite. Mesoscale rain areas produce the majority of monsoon precipitation over the Bay of Bengal (Romatschke et al. 2010). Precipitating systems over the Arabian Sea are smaller, where lower humidities limit the development of mature stratiform areas (Hirose and Nakamura 2005; Romatschke and Houze 2011a). Over the western Himalayas and mountains of Pakistan, large instabilities and drier environments favor the development of narrow, intense convective towers; MCSs are rare in this region even during the monsoon (Romatschke and Houze 2011a). Wider convective cores are observed over the central Himalayas and, at night, over the foothills and Gangetic Plain, while broad stratiform

precipitation regions are more frequent over the eastern Himalayas (Houze et al. 2007; Romatschke and Houze 2011a).

Studies from monsoon regions around the world have documented changes in convective characteristics from the pre-monsoon months to the monsoon. Zipser (1994) noted reduced lightning during the West African monsoon despite the presence of deep convective systems, including MCSs. Similarly, using TRMM observations, Kodama et al. (2005) reported more frequent lightning, higher convective rain fractions, and higher echo tops over South Asia and tropical South America during the pre-monsoon, and Yuan and Qie (2008) noted stronger vertical development of convection during the pre-monsoon over the South China Sea. The geographic distribution of convection changes during the South Asian monsoon, as the area of most intense convection and most frequent lightning and hail shifts from the Indian east coast to the western Himalayan foothills (Christian et al. 2003; Romatschke et al. 2010; Cecil and Blankenship 2012; Qie et al. 2014).

During the summer monsoon, active (rainy) and break (dry) periods are associated with propagating intraseasonal modes (Webster et al. 1977; Yasunari 1979, 1980; Webster and Chou 1980; Srinivasan et al. 1993; Singh and Kripalani 1986; Hartmann and Michelsen 1989; Webster et al. 1998; Rajeevan et al. 2010). The intraseasonal variability is typically characterized by modes in two frequency bands: ~30-60 days and ~10-30 days, with the former producing the majority of the intraseasonal variance (Krishnamurti and Subrahmanyam 1982; Hoyos and Webster 1997; Annamalai and Slingo 2001; Krishnamurthy and Shukla 2007). In the 30-60 day oscillation, an area of enhanced precipitation develops over the equatorial Indian Ocean and propagates northward, over South Asia into the Himalayas, and eastward into the western Pacific, such that the band of enhanced clouds and precipitation and the associated circulation

anomalies are oriented from northwest to southeast (Annamalai and Slingo 2001; Lawrence and Webster 2002; Hoyos and Webster 2007; Krishnamurthy and Shukla 2007; Rajeevan et al. 2010). A vertical slope is also observed, with CloudSat observations indicating increased cloud liquid water content slightly leading and increased cloud ice water content slightly lagging the precipitation maximum (Jiang et al. 2011; Rajeevan et al. 2013).

Recent work using satellite data has investigated variations in the character of precipitating systems during the intraseasonal oscillation. Analyzing TRMM data, Chattopadhyay et al. (2009) found that northward propagation is weak in the convective precipitation component but prominent in the stratiform component, which reinforces the northward propagation. The top-heavy latent heating produced by stratiform precipitation feeds back onto the large-scale pattern, forcing dynamical uplift and strengthening the monsoon trough and midlevel cyclonic circulation (Choudhury and Krishnan 2011). Over the Bay of Bengal, stratiform precipitation is predominantly associated with MCSs; individual systems propagate to the south and west while initiation locations shift northward (Zuidema 2003; Liu et al. 2008). In addition, Goswami et al. (2010) and Vellore et al. (2014) reported that extreme rainfall over the Meghalaya Plateau and eastern Himalayas is associated with mesoscale convection areas during domain-wide break (but locally rainy) intraseasonal periods. MCSs, then, play a significant role in both the propagation and the heavy precipitation episodes of the intraseasonal oscillation. However, to date no attempt has been made to quantify the intraseasonal modulation of MCS occurrence or to examine how MCS characteristics differ seasonally or with respect to the 30-60 day oscillation.

In this paper, we examine seasonal and intraseasonal variations in the geographical distribution, vertical structure, and lightning production of South Asian MCSs, focusing on sub-

regions of frequent MCS occurrence. Our analysis is based on a database of MCSs identified by Yuan and Houze (2010; hereafter, YH10) in observations from NASA's A-Train constellation (L'Ecuyer and Jiang 2010). CloudSat, also in the A-Train, carries a cloud profiling radar (CPR) that enables investigation of MCS reflectivity structures. The A-Train does not carry a lightning sensor, so lightning observations are supplied by a ground-based network.

2. Data

a. MCS identification protocol

YH10 developed a technique, summarized in Table 1, for identifying MCSs using observations from two instruments on the Aqua satellite. MCS high cloud shields are identified from Moderate Resolution Imaging Spectroradiometer (MODIS) 10.8 μm brightness temperatures (Tb_{11}), and precipitating areas are located using the Advanced Microwave Scanning Radiometer for Earth Observing System (AMSR-E) AE-Rain product (Kummerow et al. 2001; Wilheit et al. 2003; Kummerow and Ferraro 2007). Two categories of MCSs are identified:

- Separated MCSs (SMCSs), in which the precipitating area contains at most two dominant raining cores of any MCS. Most MCSs fall into this category, which is further subdivided into small SMCSs [the smallest 25%, with high cloud system (HCS; see Table 1) area <11000 km^2] and large SMCSs (the largest 25%, with HCS area >41000 km^2).
- Connected MCSs (CMCSs), in which the precipitating area contains the dominant raining cores of three or more MCSs. While A-Train satellites provide snapshots and cannot track feature development, we expect that CMCSs form through the continued upscale growth and merging of long-lived MCSs (Williams and Houze 1987; Mapes and Houze 1993).

MCSs identified using this criteria account for 57% of tropical precipitation (YH10). In this study, we analyze MCSs identified from April to November over South Asia (Fig. 1), using data from 2007-2010.

A-Train satellites operate in sun-synchronous orbit with equatorial crossings at 1:30 and 13:30 LT. Analysis of diurnal variability using TRMM indicates that over the Meghalaya Plateau and eastern Himalayas, large precipitating systems occur most frequently during early morning (3-5 LT), as nocturnal downslope winds converge with the large-scale monsoon flow, and decline to an evening minimum (20-22 LT). Over the Bay of Bengal, broad stratiform regions have a midday maximum (9-15 LT) and evening minimum (20-23 LT; Romatschke et al. 2010; Romatschke and Houze 2011a). Thus, for each region, one A-Train overpass is at or just prior to the time of peak MCS occurrence, while the other overpass is more likely to sample systems later in their lifecycle. Examination of day vs. night differences in MCS characteristics is beyond the scope of this paper.

b. CloudSat reflectivity

CloudSat's CPR measures radar reflectivity factor at 94 GHz (Stephens et al. 2002; Marchand et al. 2008). The backscatter profiles have a vertical resolution of 240 m and are available every 2.5 km along-track. Portions of each profile sampling a cloud are identified by screening for Geometric Profile (2B-GEOPROF) cloud mask values of 20 or above (Marchand et al. 2008).

Yuan et al. (2011; hereafter YHH11) identified CloudSat profiles that sampled some portion of an MCS. They then focused on anvil clouds, which they defined as having cloud base above 3 km and top above 10 km. Our approach follows Virts and Houze (2015b): we present statistics for both the precipitating and anvil regions of MCSs, where anvils are identified as in

YHH11 and the precipitating category includes all CloudSat profiles sampling the non-anvil region of the MCS.

Vertical reflectivity structures can be represented as two-dimensional histograms of reflectivity as a function of altitude, known as contoured frequency by altitude diagrams (CFADs; Yuter and Houze 1995). Cetrone and Houze (2009), YHH11, and Virts and Houze (2015b) demonstrated the use of CFADs of CloudSat observations of MCSs to infer cloud microphysical processes. Radar reflectivity can be enhanced by increased number, size, or density of particles in the radar beam. Evidence from aircraft sampling of ice particles and calculation of reflectivity at both 35 and 94 GHz by YHH11 indicates that number concentration is not the most likely reason for differences in CloudSat reflectivity observations in the upper levels of MCSs; rather, it is most likely the size of the particles. Strong updrafts prevent larger ice particles from falling out and generate supercooled water for the formation of denser graupel particles; thus, a heterogeneous reflectivity distribution including high concentrations of large reflectivities in the middle and upper troposphere indicates the CFAD was generated from CloudSat observations of precipitating systems with a convective nature. In contrast, weaker updrafts that prevail in MCS stratiform regions maintain a more homogeneous particle size distribution consisting of small ice particles that remain suspended aloft while denser particles fall out. As a result, CFADs for precipitating clouds with a stratiform character exhibit a pronounced slope, with strong modal values tending toward lower values with height in the upper troposphere. In this paper, we use the existence of a strong mode at low reflectivity sloping to lower values with height to indicate the presence of stratiform precipitation and the existence of a heterogeneous CFAD at upper levels to indicate precipitation of a more convective nature. Vertical velocities in anvils are weaker still, allowing ice particles to drift downward (Houze

2014, Chapter 6). We therefore interpret large reflectivities in anvils to indicate that the anvils are connected to active deep convective updrafts, and large particles injected into the anvils have not yet had time to fall out.

c. WWLLN lightning

Vigorous updrafts are needed to produce the rates of charge separation required for lightning (Zipser and Lutz 1994); thus, lightning is an independent indicator of convective intensity. The World Wide Lightning Location Network (WWLLN) monitors very low frequency (VLF) lightning sferics, locating lightning to within ~5 km and <10 μs (Abarca et al. 2010). WWLLN's global detection efficiency during the period of this study is estimated to be ~10% of cloud-to-ground lightning with current stronger than ±35 kA (Rodger et al. 2009; Abarca et al. 2010; Rudlosky and Shea 2013).

MCS lightning production is calculated as follows: for each MCS, a $0.25° \times 0.25°$ grid is defined with the center of the largest raining core of the MCS at (0°, 0°) relative latitude and longitude, and grid boxes containing some portion of the MCS cloud shield are identified. WWLLN lightning observations from a one-hour window centered on the MODIS overpass are assigned to the relative latitude-longitude grid based on their location relative to the MCS. The total number of lightning strokes during the one-hour observation window in grid boxes affected by the MCS is termed the MCS lightning production.

Independent lightning production values were calculated for MCS-like precipitation features observed by TRMM and selected using the criteria of Virts and Houze (2015a; their Section 2d). Seasonal and intraseasonal variations in the TRMM-based statistics (not shown) are qualitatively consistent with those presented in this paper.

d. ERA-Interim

Atmospheric conditions are represented by fields from the European Centre for Medium-Range Weather Forecasting (ECMWF) interim re-analysis (ERA-Interim; Dee et al. 2011), with the 6-hourly fields (3-hourly for CAPE) averaged to create daily values at each grid point. The results in this paper are based on 1.5° or, when indicated, one-eighth degree resolution. Anomalies are calculated with reference to the JJAS-mean.

e. BSISO index

The Boreal Summer Intraseasonal Oscillation (BSISO) indices developed by Lee et al. (2013) represent the strength and evolution of the 30-60 and 10-30 day modes. The indices are based on multivariate empirical orthogonal function (EOF) analysis of daily anomalies of OLR and 850-hPa zonal winds over the south and southeast Asian monsoon regions. The first two EOFs, whose principal component (PC) time series are collectively designated BSISO1, represent northward propagation from the equatorial Indian Ocean to southern Asia at 30-60 day time scales. The third and fourth PCs (designated BSISO2) are associated with northward propagation at 10-30 day time scales and exhibit peak variability around the time of monsoon onset. For this study, eight phases of BSISO1 and BSISO2 are defined as in Lee et al. (2013), and each day during JJAS is assigned to whichever phase of each index it projected onto most strongly. Days on which the magnitude of the BSISO index was less than one standard deviation from zero (about 15% of all JJAS days) are discarded.

Similar results to those presented in this paper are obtained with alternate indices of the 30-60 variability such as the BSISO index of Kikuchi et al. (2012) or the monsoon intraseasonal oscillation (MISO) index of Shukla (2014). We chose the Lee et al. (2013) index because it also tracks a component of 10-30 day variability.

3. Seasonal variability of atmospheric conditions

In this study, we focus on three seasons: the summer monsoon [June-September (JJAS)] and the shoulder seasons, the pre-monsoon [April-May (AM)] and post-monsoon [October-November (ON)]. Strong daytime heating of land during the pre-monsoon creates conditionally unstable conditions favorable for intense convection (Romatschke and Houze 2011b). Vigorous diurnally-driven convection produces lightning maxima along the southwest coast of India and the west coast of Burma as well as over the Meghalaya Plateau and the Himalayas (Fig. 2). Precipitation maxima are similarly distributed but less prominent than the lightning.

During the monsoon, a low-pressure trough extends from northwest to southeast over northern India, while weak ridging is observed along the west coast (Fig. 2b). The associated westerly winds over the eastern Arabian Sea and southwesterly winds over the Bay of Bengal advect moist air over South Asia, producing frequent and sometimes heavy precipitation. While precipitation is concentrated over and upstream of the mountains (Grossman and Durran 1984; Houze et al. 2007), monsoon lightning exhibits a markedly different distribution, with maxima over eastern India and extending along the Himalayas. Upper-tropospheric winds are easterly, such that monsoon convection experiences strong shear (Johnson and Houze 1987).

The transition between the summer and winter monsoons can be seen in the October-November means (Fig. 2c). Southwesterly flow gives way to weak northeasterlies. Without the moist advection by monsoon winds, precipitation over South Asia decreases except over extreme southern India. As in the pre-monsoon, post-monsoon lightning is most frequent along the west coasts of southern India, Sri Lanka, and Burma.

4. Seasonal variability of MCSs

a. Variability of MCS distribution

Pre-monsoon small SMCSs are scattered over the eastern terrain (Fig. 3a). Large SMCSs occur frequently over the Meghalaya Plateau but rarely elsewhere over land. Both large and connected MCSs are observed over the Bay of Bengal, particularly the southeastern coastal waters. MCSs of all types are observed over the near-equatorial Indian Ocean.

MCSs are most frequent during the monsoon (Fig. 3b). Hotspots of small SMCSs are observed along the Himalayas and eastern terrain, particularly over the northeastern notch, while large SMCSs are more evenly distributed along the Himalayas and the Indian west and east coasts. Large SMCSs are ubiquitous over most of the Bay of Bengal. The merging of these large systems into CMCSs is most frequent over the northern and eastern bay and seems to be enhanced by proximity to the mountainous Burma coast. Close inspection reveals that the occurrence of large SMCSs extends over the near-coastal land regions of Bangladesh and Burma, while CMCSs occur discernably upstream of land. There is a secondary maximum in large and connected MCS occurrence over the eastern Arabian Sea, upstream of the Western Ghats, again indicating that their occurrence is enhanced upstream of mountains. Romatschke et al. (2010) also noted more broad stratiform regions over the Bay of Bengal compared to the Arabian Sea and hypothesized that lower humidities over the Arabian Sea limited the formation of mature stratiform areas.

The retreat of the monsoon is associated with decreased MCS occurrence over most of the domain (Fig. 3c). Post-monsoon MCSs are located primarily over the southeastern Arabian Sea and outlining the Bay of Bengal, with some large systems extending into southern India and southern Bangladesh.

Spatial patterns of precipitation and large and connected MCSs are similar for each season, although precipitation maxima are more closely tied to coastlines and topography than the MCSs (Fig. 2-3; Biasutti et al. 2012). Romatschke et al. (2010) suggested that large MCSs are the primary precipitation producers during the monsoon. Here, we further suggest that while MCSs occur less frequently during the shoulder seasons, they are still major producers of precipitation. Pre-monsoon lightning and large MCSs both have maxima offshore of southern India and Sri Lanka, over the eastern Bay of Bengal, and over the Meghalaya Plateau. Their distributions exhibit weaker parallels during the post-monsoon and are generally dissimilar during the monsoon, suggesting that MCS lightning contributions are most significant during the pre-monsoon.

b. Variability of MCS characteristics

Cetrone and Houze (2009) and YHH11 presented CFADs for the anvils of MCSs over the Bay of Bengal and the Indian Ocean sector, respectively, emphasizing variations in the reflectivity distributions as a function of anvil thickness and distance from the MCS center. Subsequently, Virts and Houze (2015b) investigated vertical structures of both the precipitating and anvil regions of all tropical MCSs, stratified by MCS type. Here, we narrow our focus to MCSs over three regions: the Bay of Bengal, the Meghalaya Plateau, and the northeast Himalayan notch (Fig. 1).

1. BAY OF BENGAL

Seasonal CFADs for the precipitating portions of Bay of Bengal MCSs are shown in Fig. 4. The smaller sample size leads to noisier distributions than in Virts and Houze (2015b), but the basic characteristics can still be seen. Below the melting layer (indicated by the vertical discontinuity around 5 km), reflectivities decrease as the signal is attenuated by precipitation.

Above the melting layer, the reflectivity distribution in small SMCSs exhibits a convective character, indicated (Section 2b) by heterogeneity in the CFAD, including large reflectivities in the mid and upper troposphere. In contrast, large and connected MCSs exhibit a more stratiform character, with reflectivity distributions sloping toward lower values with height in the upper troposphere.

Pre-monsoon large and connected Bay of Bengal MCSs are more convective than monsoon MCSs, indicated by the high reflectivities extending to ~13 km compared to ~10 km during the monsoon (Fig. 4), while monsoon MCSs exhibit a stronger stratiform character. This contrast is confirmed in the difference plots (Fig. 4d), which show that high reflectivities aloft are more prevalent in pre-monsoon MCSs, consistent with previous observations of changes in the characteristics of precipitating systems from the pre-monsoon to monsoon seasons (see Section 1). Note that this contrast is observed for each MCS type; i.e., even the largest MCSs have a greater convective character during the pre-monsoon.

Similarly, higher reflectivities are observed in the anvils of large and connected pre-monsoon Bay of Bengal MCSs (Fig. 5). Monsoon MCS anvils have generally lower reflectivities, consistent with the development of extensive, mature anvils with weak ascent. Anvils during the monsoon are generally thicker than in the shoulder seasons.

Post-monsoon Bay of Bengal MCSs exhibit reflectivity distributions between those of the pre-monsoon and monsoon MCSs, appearing somewhat more convective than monsoon MCSs but not as convective as the pre-monsoon MCSs (Fig. 4-5).

Independent confirmation of seasonal differences in updraft intensity in MCSs is provided by the lightning production (Fig. 6). For each MCS type, lightning production decreases significantly from the pre-monsoon to monsoon season. This behavior is particularly

apparent in large and connected MCSs, in which lightning production decreases by a factor of ~3-4 during the monsoon, slightly larger than the factor of ~2 decrease reported by Yuan and Qie (2008) based on TRMM observations of MCSs over the South China Sea. For each MCS type, lightning production remains low during the post-monsoon and is not statistically different from that during the monsoon.

2. MEGHALAYA PLATEAU

Compared to the Bay of Bengal, there are fewer MCSs over the Meghalaya Plateau, particularly during the post-monsoon (Fig. 3). Thus, we focus on pre-monsoon and monsoon MCSs and do not stratify the statistics by MCS type.

Pre-monsoon Meghalaya Plateau MCSs exhibit a strongly convective nature, with peak reflectivities above 10 dBZ in the mid-troposphere (Fig. 7). The lack of noticeable modal decrease in reflectivity with height in the upper troposphere in the precipitating region and the noisy appearance of the anvil CFAD indicates that the MCSs have not developed mature stratiform or anvil regions.

Monsoon MCSs over the Meghalaya Plateau exhibit markedly different characteristics. Their precipitating regions are generally taller than those in pre-monsoon MCSs; however, peak reflectivities are concentrated below the 0°C level, suggesting both the maritime-tropical origin of the airmass (Houze et al. 2007) and orographic enhancement (see Section 7). As over the Bay of Bengal, monsoon MCSs over the Meghalaya Plateau exhibit more mature stratiform reflectivity structures than those during the pre-monsoon. The narrow reflectivity distribution in their anvils indicates the development of more uniform, weaker ascent. In agreement with these observations, MCS lightning production in this region decreases by almost a factor of two during the monsoon (not shown).

3. NORTHEAST HIMALAYAN NOTCH

Few MCSs are observed over the northeast Himalayan notch during the shoulder seasons (Fig. 3). Monsoon MCSs in this region are generally shorter than those over the Meghalaya Plateau and Bay of Bengal, and their reflectivity structures, while robust, do not exhibit the pronounced stratiform signature observed in the other regions. The broad distribution of the anvil reflectivities in northeast Himalayan notch MCSs indicates that size sorting and aggregation processes are not as developed in these systems, and there is a greater concentration of larger reflectivities (>0 dBZ) than in other regions or seasons. These results indicate that monsoon MCSs in this region are predominantly small (Fig. 3) and convective, with some large ice particles detrained into their anvils. MCS lightning production in this region is low and not significantly distinct in any season (not shown). The absence of a local maximum over this region in the seasonal lightning climatology (Fig. 2b) suggests that updrafts in these MCSs are typically not vigorous enough for significant electrification. TRMM observations indicate a local maximum in broad stratiform precipitation features over the eastern Himalayas during the pre-monsoon and monsoon (Houze et al. 2007; Romatschke and Houze 2011a, b); our results suggest that these are predominantly orographically-driven features that lack the convective character necessary to be classified as an MCS.

5. Atmospheric conditions associated with MCS occurrence

Having examined the seasonal variability of MCSs over South Asia, we now focus on the monsoon season (June-September), when MCS occurrence peaks. 925-hPa geopotential height and wind anomalies on days with a large or connected MCS over the Bay of Bengal are shown in Fig. 9. The patterns are qualitatively similar, with an anomalous low over the northwestern Bay

and associated cyclonic wind anomalies. Strengthening of this pattern evidently favors the merging of MCSs to form CMCSs. Lag composites (not shown) indicate that the lows propagate northwestward over land on subsequent days, as is typical for Bay of Bengal depressions (e.g., Shukla 1978). This observation concurs with previous evidence that MCSs are associated with synoptic-scale Bay of Bengal depressions (Houze and Churchill 1987; Houze et al. 2007; Romatschke et al. 2010). The anomaly patterns in Fig. 9 are domain-wide: both the southwesterly monsoon flow over the Arabian Sea and easterly flow along the Himalayas are strengthened, and there is a weaker secondary low over northwest India. The relationship between Bay of Bengal MCSs and the large-scale intraseasonal oscillation is investigated in Section 7.

Lower-tropospheric anomalies associated with Meghalaya Plateau MCSs (Fig. 10) are nearly opposite to those for Bay of Bengal MCSs. Anomalous high pressure and anticyclonic circulation are centered over the head of the Bay. Winds over the Meghalaya Plateau, which are southerly in the seasonal-mean (Fig. 2), are strengthened and have a stronger southwesterly component on MCS days, increasing the flow of moisture from the Bay of Bengal and the Bangladesh wetlands (Medina et al. 2010). Previous studies have also noted that anomalously southwesterly winds favor heavy precipitation events over the plateau (Romatschke and Houze 2011a; Sato 2013).

In contrast to the other two sub-regions, the large-scale anomaly pattern on days with northeast Himalayan notch MCSs is nondescript, with weak easterly anomalies to the southwest (Fig. 11). Zooming in at one-eighth degree resolution, a mesoscale low and associated cyclonic wind anomalies can be seen over the Irriwaddy Valley. The low is slightly south of the small SMCS hotspot (Fig. 3b), which is collocated with maximum anomalous CAPE (Fig. 11c). We

conclude that the mean JJAS pattern, in which moist air from the Bay of Bengal is advected up the valley toward the mountains, combined with locally enhanced CAPE, favors MCS occurrence in this region.

6. 30-60 day variability of atmospheric conditions

Lower-tropospheric anomalies during eight phases of the BSISO1 index (i.e., the 30-60 day mode) are shown in Fig. 12. During phases 1-2, an anomalous high and associated anticyclonic circulation are centered over the northern Bay of Bengal and stretch northwestward across India. Lower heights at the southern edge of the domain intensify and propagate northward during phases 3-5, occupying most of the domain. The associated wind shift amplifies the monsoon southwesterlies over the Arabian Sea and southeasterlies over the Himalayan foothills (Fig. 2). Over much of the Bay of Bengal, winds are anomalously westerly during phases 5-6, as the low peaks in intensity at the head of the Bay. The low extends along the Himalayas during phases 7-8, and an anomalous high shifts northward from the equator to the Indian west coast.

As discussed in Section 1, monsoon intraseasonal variability is often described as producing active and break periods. Here, we designate BSISO1 phases 4-7 as the active period, with anomalous low pressure over the Indian subcontinent and general strengthening of the monsoon circulation, and phases 8-3 as the break period.

During the active period, enhanced precipitation extends from the northeastern Arabian Sea southeastward across India and the Bay of Bengal (Fig. 13), in agreement with previous studies based on rain gauge data (Singh and Kripalani 1986; Hartmann and Michelsen 1989; Krishnamurthy and Shukla 2007; Rajeevan et al. 2010). These active periods produce ~70% of

summer precipitation over the Bay (Hoyos and Webster 2007). The largest precipitation anomalies in Fig. 13 are over the southeastern Bay, where anomalous westerly winds meet the coast. The rainy anomalies are flanked by bands of suppressed precipitation that extend from the southeastern Arabian Sea toward the Maritime Continent and also along the eastern Himalayas. Enhanced lightning anomalies are also oriented roughly northwest to southeast. However, within this band of active-period enhancement, the locations of lightning maxima are negatively correlated with the locations of the precipitation maxima, and the lightning zone is somewhat broader. The peak of lightning enhancement over the Eastern Ghats and the western Bay of Bengal is associated with enhanced CAPE (not shown).

7. 30-60 day variability of MCSs

a. Variability of MCS distribution

MCSs are ubiquitous over the northern and middle Bay of Bengal during the active period (Fig. 14). Large SMCSs are more concentrated over the northern and southeastern bay, while CMCSs are enhanced throughout the northeastern bay. Difference plots (Fig. 14c) show enhanced occurrence of large and connected MCSs extending from the northeastern Arabian Sea southeastward across the Bay of Bengal during the active period, flanked by suppressed anomalies, similar to the precipitation pattern (Fig. 13). In contrast, the distribution of small SMCSs is patchy during both active and break periods, with hotspots scattered primarily over the Himalayas and eastern terrain. No coherent spatial pattern is observed in the difference plot for small SMCSs. Comparison of Fig. 13 and 14 suggests that, so far as the precipitating cloud population is concerned, monsoon intraseasonal variability is primarily evident in the modulated occurrence of large and connected MCSs. The modulation of large SMCSs most closely mirrors

the rainfall modulation; CMCSs likely form over the Bay of Bengal because the moist environment favors longer lifetimes and greater probability that systems will merge. Examining TRMM data during the monsoon, Chattopadhyay et al. (2009) observed prominent, organized propagation of the stratiform precipitation component at 30-60 day timescales but only weak propagation of convective precipitation. Our results support their conclusion and further suggest that the stratiform precipitation is primarily associated with large MCSs over land and both large and connected MCSs over the Bay of Bengal.

The number of MCSs observed over each sub-region during each BSISO1 phase is shown in Fig. 15. Prominent variations of a factor of 2-3 are observed over the Meghalaya Plateau and Bay of Bengal, with peak occurrence at the end of the break period (phases 2-3) and at the peak of the active period (phase 5), respectively. Comparison with Fig. 9-10 confirms that the large-scale patterns associated with MCS occurrence in these regions resemble the corresponding BSISO1 anomalies. Northeast Himalayan notch MCSs also appear to peak during phases 2-3; however, the large-scale anomalies associated with these MCSs are weak (Fig. 11) and do not resemble the BSISO1 pattern. For this reason, we do not further investigate BSISO1 modulation of northeast Himalayan notch MCSs.

b. Variability of MCS characteristics

In the remainder of this section, we examine how MCS characteristics vary during the 30-60 day oscillation. For each reference box, the regional-mean TRMM 3B42 rain rate is calculated for each BSISO1 phase. The four successive phases containing the peak precipitation are designated as the local "rainy" period and the remaining four phases as the "dry" period. Note that the local rainy period over the Bay of Bengal matches the active monsoon period

(phases 4-7), while the local rainy period over the Meghalaya Plateau occurs in break conditions (phases 8-3), in association with the southwesterly flow around the high (Fig. 12).

1. BAY OF BENGAL

Reflectivity structures for MCSs during the local rainy and dry periods are shown in Fig. 16-17. The intraseasonal differences are more subtle than the seasonal differences (Fig. 4-5). Difference CFADs indicate slightly higher mid-tropospheric reflectivities in the precipitating regions of rainy period MCSs, while in the upper troposphere, higher reflectivities suggest deeper updrafts and increased lofting of larger ice particles in dry period MCSs. These contrasts are also observed in the anvil CFADs, particularly in CMCSs.

Lightning production of Bay of Bengal MCSs decreases during phase 2 and remains lower through the rainy period before increasing at the beginning of the dry period (Fig. 18b). Increased lightning during the dry period is consistent with the stronger updrafts suggested by the reflectivity structures. Note, however, that just as the intraseasonal contrasts in MCS reflectivity structures are not as pronounced as those between pre-monsoon and monsoon MCSs, intraseasonal variations in MCS lightning, while statistically significant, are not as robust as the seasonal differences (Fig. 6).

At first glance, the results in Fig. 18b appear contradictory to observations of overall increased lightning over the Bay of Bengal during the active period (Fig. 13). Decreased lightning production in individual MCSs is partially offset by the sharp increase in MCS occurrence during the active period. In addition, lightning frequency increases most over the western Bay, where there are comparatively fewer MCSs (Fig. 14). This suggests that isolated convection may be responsible for the increased lightning.

2. MEGHALAYA PLATEAU

The vertical reflectivity structures of Meghalaya Plateau MCSs exhibit marked differences during locally rainy and dry periods (Fig. 19). In the precipitating regions of locally dry (active monsoon) period MCSs, the distribution is diffuse below the melting layer but narrowly peaked at higher reflectivities (>10 dBZ) in the middle and upper troposphere. MCSs during both the pre-monsoon and locally dry period exhibit an intense convective character (Fig. 7). Locally dry period MCSs are somewhat taller, however, and their anvils are more robust, with higher reflectivities than in pre-monsoon MCSs.

In contrast, during the break monsoon (locally rainy) period, the CFAD maximum is in the lower troposphere, consistent with strong orographic enhancement of the precipitation as moist air advection is strengthened in connection with the anomalous southwesterly flow riding up onto the plateau (Fig. 10). The distribution is broad in the mid-troposphere but narrows with height in the upper troposphere, indicating the presence of more mature stratiform rain areas. These contrasts are highlighted in the difference plot in Fig. 19c, where the sign switches around 5 km.

Lightning production in Meghalaya Plateau MCSs varies intraseasonally (Fig. 18a), increasing by about a factor of four at the end of the locally rainy period. This result is only marginally statistically significant, perhaps due to the small sample size (note the large error bars).

9. Conclusions

Characteristics of MCSs over the South Asian monsoon region vary by geographic location, by season, and intraseasonally during the monsoon. Small SMCSs are concentrated over the Himalayas and the complex eastern terrain. Large and connected MCSs occur most

frequently over the Bay of Bengal, and analysis of CloudSat radar reflectivity vertical structures shows that they are less convective than land MCSs and develop more mature stratiform precipitation areas (Fig. 4, 7-8), consistent with the broad land/ocean contrasts in MCS anvil characteristics observed by YHH11.

a. Seasonal variation of MCS structure

Isolated convection dominates over much of the South Asian landmass during the pre-monsoon, in part because dry environments limit the development of large stratiform areas (Romatschke et al. 2010; Romatschke and Houze 2011b). Moist advection toward the Meghalaya Plateau (Fig. 2a) permits some convection to organize into MCSs with an intense convective character, with updrafts lofting large graupel and ice particles into the upper portions of the systems, producing frequent lightning and only small anvils (Fig. 7). Bay of Bengal MCSs are also more convective during the pre-monsoon (Fig. 4-5). Pre-monsoon MCS lightning production is significantly larger than during the monsoon; this contrast is most significant in large and connected MCSs (Fig. 6).

During the monsoon, MCSs are the major precipitation producers, especially over the Bay of Bengal, central and eastern Himalayas, and Meghalaya Plateau. A weaker maximum in MCS occurrence is located over the eastern Arabian Sea, upstream of the Western Ghats. The vertical reflectivity structures of monsoon MCSs over the Bay of Bengal and Meghalaya Plateau are consistent with mesoscale ascent in mature stratiform precipitation areas and further size sorting in their anvils, indicated by a strong decrease of reflectivity with height in the upper troposphere (Fig. 4-5, 7). Consistent with past studies, reanalysis composites show that Bay of Bengal MCSs are strongly associated with Bay of Bengal depressions (Fig. 9). Meghalaya Plateau MCSs are much different, exhibiting strong orographic enhancement and occurring on

days when anomalous southwesterly winds strengthen the moist air advection from the Bay of Bengal up the slopes of the plateau (Fig. 10).

During the post-monsoon, the tropical convergence zone moves southward, and winds over South Asia begin to shift to the northeasterlies of the winter monsoon (Fig. 2c). Post-monsoon MCSs are primarily observed over the Bay of Bengal and near-equatorial belt, and rarely attain large size over land (Fig. 3). The reflectivity structures of these MCSs are more convective than those of the monsoon but more stratiform than those of the pre-monsoon (Fig. 4-5), and their lightning production remains lower than in pre-monsoon MCSs (Fig. 6). Overall, our results indicate a fundamental regime change from pre-monsoon to monsoon, while the post-monsoon season appears to be a waning of the monsoon.

Northeast Himalayan notch MCSs exhibit markedly different characteristics than those over the neighboring Meghalaya Plateau. MCS formation during the monsoon is favored on days with locally enhanced CAPE, when the large-scale pattern resembles the seasonal mean (Fig. 11). The broad stratiform areas observed in this region in previous studies (Romatschke et al. 2010) evidently do not match the MCS criteria, and those features identified as MCSs are generally small and convective (Fig. 3, 8). Further investigation is needed into the characteristics and formation mechanisms of precipitating features in this region.

b. Intraseasonal variations in MCS structure

A northward-propagating intraseasonal (30-60 day) mode modulates the monsoon circulation. No clear modulation of small SMCS occurrence is observed in connection with this intraseasonal mode; however, large and connected MCSs and their characteristics do vary in relation to the 30-60 day mode. During the active period, the southwesterlies over the Arabian Sea are strengthened, and low pressure over the northern Bay of Bengal is associated with

anomalously strong westerly flow over the Bay and easterlies along the Himalayas (Fig. 12). Enhanced precipitation, lightning, and large and connected MCS occurrence extend from the northeastern Arabian Sea southeastward across the Bay of Bengal, flanked by anomalies of opposite sign (Fig. 13-14). However, within this zone of enhancement, lightning, MCS, and rainfall maxima are not collocated. Large SMCS occurrence mirrors precipitation occurrence over both land and ocean, but CMCS anomalies are mainly over the Bay of Bengal. In addition, lightning (interpreted here as a proxy for the degree of convective nature of the precipitating systems) is anti-correlated with large MCS and rainfall occurrence. That is, in the active monsoon zone, both lightning and MCS occurrence are enhanced but not in the same locations.

The characteristics of large and connected MCSs are also modulated by the 30-60 day oscillation, and the form of the modulation varies strongly by region. Over the Bay of Bengal, the locally rainiest period coincides with the domain-wide active period. MCSs over the Bay during this period exhibit slightly more stratiform reflectivity structures and decreased lightning production (Fig. 16-18). Over the Meghalaya Plateau, however, the locally rainiest period and peak MCS occurrence are during the domain-wide break period, and the locally driest period coincides with the large-scale active period. The reason for this apparent incongruity is that the high pressure anomaly during the large-scale break period strengthens southwesterly flow up the slope of the Plateau, leading to orographic lifting and convective triggering (Fig. 10). The strong orographic enhancement in the JJAS-mean CFADs for this region (Fig. 7) is observed only in MCSs during the locally rainy (large-scale break) period. CFADs for Meghalaya Plateau MCSs during the locally dry period indicate the presence of large ice and graupel particles in the upper troposphere in the precipitating region and being incorporated into the anvils (Fig. 19), consistent with a sharp increase in lightning production (Fig. 18).

c. Dry versus moist large-scale environments

Some parallels are observed between MCSs occurring in pre-monsoon vs. monsoon seasons and locally dry vs. rainy periods within the monsoon season. For example, the strongly convective characteristics of Meghalaya Plateau MCSs during the active monsoon (locally dry) period are quite similar to the pre-monsoon MCSs (Fig. 7, 19). Lightning production during that period, while uncertain due to small sample size, may be even larger than during the pre-monsoon (Fig. 19). Over the Bay of Bengal, contrasts in MCS structure between locally rainy and dry periods are similar to those between the monsoon and pre-monsoon seasons, but muted (compare Fig. 4d, 5d and 16c, 17c).

d. Comparison to MJO MCSs

Parallels are also observed between variations in MCS characteristics during BSISO1 and the Madden-Julian Oscillation (MJO; Zhang 2005), which also varies at 30-60 day timescales but is prominent in the equatorial belt during boreal winter. MCS behavior during the MJO was examined by Virts and Houze (2015a). The active periods of both oscillations are associated with increased occurrence of large and connected MCSs and with decreased MCS lightning production. Virts and Houze (2015a) also noted larger convective rain fractions in MCS-like features observed by TRMM during the MJO break period, consistent with our observation of more convective CFADs during the BSISO1 break period. These parallels in the monsoon and MJO contexts illustrate the fundamental control of convective and mesoscale behavior by the large-scale environment.

e. 10-30 day variability

As discussed in Section 1, previous studies have reported 10-30 day variability during the monsoon. Preliminary examination indicates that MCS occurrence and characteristics do not

vary significantly with the northward-propagating 10-30 day mode as represented by BSISO2 (see the online supplement to this paper). A westward-propagating 10-30 day oscillation has also been documented during the summer monsoon, originating in the tropical western Pacific and associated with Rossby wave propagation (Annamalai and Slingo 2001). This mode is prominent during mid-summer (Annamalai and Slingo 2001) and is primarily contained in the 25-80 day band (Hoyos and Webster 2007). Sato (2013) and Hatsuzuka et al. (2014) linked the 10-30 day oscillation with heavy precipitation events over Bangladesh and the Meghalaya Plateau; they also noted the mesoscale organization of the convection. Thus, investigation of MCS variability with the westward-propagating 10-30 day oscillation is warranted.

Acknowledgments

The authors thank Beth Tully for her expert processing of the graphics and three reviewers for their helpful comments. This work was supported by the National Aeronautics and Space Administration (grant NNX13AQ37G) and the U.S. Department of Energy (grant DE-SC008452). Lightning location data were provided by WWLLN (http://wwlln.net), a collaboration of over 50 universities and institutions. ERA-Interim data are available from the European Centre for Medium-Range Weather Forecasts (http://ecmwf.int/); CloudSat data are avilable from the CloudSat Data Processing Center (http://www.cloudsat.cira.colostate.edu); and MODIS, AMSR-E, and TRMM data are available from the NASA data centers (http://ladsweb.nascom.nasa.gov/, http://nsidc.org/data/amsre, and http://mirador.gsfc.nasa.gov, respectively).

References

Abarca, S. F., K. L. Corbosiero, and T. J. Galarneau, Jr., 2010: An evaluation of the Worldwide Lightning Location Network (WWLLN) using the National Lightning Detection Network (NLDN) as ground truth. *J. Geophys. Res.*, **115**, D18206, doi:10.1029/2009JD013411.

Annamalai, H., and J. M. Slingo, 2001: Active/break cycles: diagnosis of the intraseasonal variability of the Asian summer monsoon. *Clim. Dyn.*, **18**, 85-102.

Biasutti, M., S. E. Yuter, C. D. Burleyson, and A. H. Sobel, 2012: Very high resolution rainfall patterns measured by TRMM precipitation radar: seasonal and diurnal cycles. *Clim. Dyn.*, **39**, 239-258, doi:10.1007/s00382-011-1146-6.

Cecil, D. J., and C. B. Blankenship, 2012: Toward a global climatology of severe hailstorms as estimated by satellite passive microwave imagers. *J. Climate*, **25**, 687-703, doi:10.1175/JCLI-D-11-00130.1.

Cetrone, J., and R. A. Houze, Jr., 2009: Anvil clouds of tropical mesoscale convective systems in monsoon regions. *Quart. J. Roy. Met. Soc.*, **135**, 305-317, doi:10.1002/qj.389.

Chattopadhyay, R., B. N. Goswami, A. K. Sahai, and K. Fraedrich, 2009: Role of stratiform rainfall in modifying the northward propagation of monsoon intraseasonal oscillation. *J. Geophys. Res.*, **114**, D19114, doi:10.1029/2009JD011869.

Choudhury, A. D., and R. Krishnan, 2011: Dynamical response of the South Asian monsoon trough to latent heating from stratiform and convective precipitation. *J. Atmos. Sci.*, **68**, 1347-1363, doi:10.1175/2011JAS3705.1.

Christian, H. J., and Coauthors, 2003: Global frequency and distribution of lightning as observed from space by the Optical Transient Detector. *J. Geophys. Res.*, **108**, No. D1, 4005, doi:10.1029/2002JD002347.

Dee, D. P., and Coauthors, 2011: The ERA-Interim reanalysis: configuration and performance of the data assimilation system. *Quart. J. Roy. Met. Soc.*, **137**, 533-597, doi:10.1002/qj.828.

Goswami, B. B., P. Mukhopadhyay, R. Mahanta, and B. N. Goswami, 2010: Multiscale interaction with topography and extreme rainfall events in the northeast Indian region. *J. Geophys. Res.*, **115**, D12114, doi:10.1029/2009JD012275.

Grossman, R. L., and D. R. Durran, 1984: Interaction of low-level flow with the Western Ghat Mountains and offshore convection in the summer monsoon. *Mon. Wea. Rev.*, **112**, 652-672.

Hartmann, D. L., and M. L. Michelsen, 1989: Intraseasonal periodicities in Indian rainfall. *J. Atmos. Sci.*, **46**, 2838-2862.

Hatsuzuka, D., T. Yasunari, and H. Fujinami, 2014: Characteristics of low pressure systems associated with intraseasonal oscillation of rainfall over Bangladesh during boreal summer. *Mon. Wea. Rev.*, **142**, 4758-4774, doi:10.1175/MWR-D-00307.1.

Hirose, M., and K. Nakamura, 2005: Spatial and diurnal variation of precipitation systems over Asia observed by the TRMM precipitation radar. *J. Geophys. Res.*, **110**, D05106, doi:10.1029/2004JD004815.

Houze, R. A., Jr., 2014: *Cloud Dynamics*, *2nd ed.*, Elsevier, 432 pp.

Houze, R. A., Jr., and D. D. Churchill, 1987: Mesoscale organization and cloud microphysics in a Bay of Bengal depression. *J. Atmos. Sci.*, **44**, 1845-1867.

Houze, R. A., Jr., D. C. Wilton, and B. F. Smull, 2007: Monsoon convection in the Himalayan region as seen by the TRMM precipitation radar. *Quart. J. Roy Meteor. Soc.*, **133**, 1389-1411, doi:10.1002/qj.106.

Hoyos, C. D., and P. J. Webster, 2007: The role of intraseasonal variability in the nature of Asian monsoon precipitation. *J. Climate*, **20**, 4402-4424, doi:10.1175/JCLI4252.1.

Johnson, R. H., and R. A. Houze, Jr., 1987: Precipitating cloud systems of the Asian monsoon. *Monsoon Meteorology*, ed. C.-P. Chang and T. N. Krishnamurti, Oxford University Press, 560 pp.

Kodama, Y.-M., A. Ohta, M. Katsumata, S. Mori, S. Satoh, and H. Ueda, 2005: Seasonal transition of predominant precipitation type and lightning activity over tropical monsoon areas derived from TRMM observations. *Geophys. Res. Lett.*, **32**, L14710, doi:10.1029/2005GL022986.

Krishnamurthy, V., and J. Shukla, 2007: Intraseasonal and seasonally persisting patterns of Indian monsoon rainfall. *J. Climate*, **20**, 3-20, doi:10.1175/JCLI3981.1.

Krishnamurti, T. N., and D. Subrahmanyam, 1982: The 30-50 day mode at 850 mb during MONEX. *J. Atmos. Sci.*, **39**, 2088-2095.

Kummerow, C., and R. Ferraro, 2007: EOS/AMSR-E level-2 rainfall. National Snow and Ice Data Center Algorithm Theoretical Basis Doc., 10 pp. [Available online at http://nsidc.org/data/amsre/pdfs/amsr_atbd_supp06_L2_rain.pdf.]

Kummerow, C., and Coauthors, 2001: The evolution of the Goddard profiling algorithm (GPROF) for rainfall estimation from passive microwave sensors. *J. Appl. Meteor.*, **40**, 1801-1820.

Lawrence, D. M., and P. J. Webster, 2002: The boreal summer intraseasonal oscillation: Relationship between northward and eastward movement of convection. *J. Atmos. Sci.*, **59**, 1593-1606.

L'Ecuyer, T. S., and J. H. Jiang, 2010: Touring the atmosphere aboard the A-Train. *Physics Today*, **63**, 36-41, doi:10.1063/1.3463626.

Lee, J.-Y., B. Wang, M. C. Wheeler, X. Fu, D. E. Waliser, and I.-S. Kang, 2013: Real-time multivariate indices for the boreal summer intraseasonal oscillation over the Asian summer monsoon region. *Clim. Dyn.*, **40**, 493-509.

Liu, C., M. W. Moncrieff, and J. D. Tuttle, 2008: A note on propagating rainfall episodes over the Bay of Bengal. *Quart. J. Roy. Meteor. Soc.*, **134**, 787-792, doi:10.1002/qj.246.

Mapes, B. E., and R. A. Houze, Jr., 1993: Cloud clusters and superclusters over the oceanic warm pool. *Mon. Wea. Rev.*, **121**, 1398-1415, doi:10.1175/1520-0493(1993)121<1398:CCASOT>2.0.CO;2.

Marchand, R., G. G. Mace, T. Ackerman, and G. Stephens, 2008: Hydrometeor detection using CloudSat—an earth-orbiting 94-GHz cloud radar. *J. Atmos. Oceanic Tech.*, **25**, 519-533, doi:10.1175/2007JTECHA1006.1.

Medina, S., R. A. Houze, Jr., A. Kumar, and D. Niyogi, 2010: Summer monsoon convection in the Himalayan region: Terrain and land cover effects. *Quart. J. Roy. Meteor. Soc.*, **136**, 593-616, doi:10.1002/qj.601.

Qie, X., X. Wu, T. Yuan, J. Bian, and D. Lu, 2014: Comprehensive pattern of deep convective systems over the Tibetan Plateau-South Asian monsoon region based on TRMM data. *J. Climate*, **27**, 6612-6626, doi:10.1175/JCLI-D-14-0076.1.

Rajeevan, M., P. Rohini, K. Niranjan Kumar, J. Srinivasan, and C. K. Unnikrishnan, 2013: A study of vertical cloud structure of the Indian summer monsoon using CloudSat data. *Clim. Dyn.*, **40**, 637-650, doi:10.1007/s00382-012-1374-4.

Ramage, C. S., 1971: *Monsoon Meteorology*. Academic Press, New York, 296 pp.

Rodger, C. J., J. B. Brundell, R. H. Holzworth, E. H. Lay, N. B. Crosby, T.-Y. Huang, and M. J. Rycroft, 2009: Growing detection efficiency of the World Wide Lightning Location Network. *AIP Conference Proceedings*, 15-20, doi:10.1063/1.3137706.

Romatschke, U., and R. A. Houze, Jr., 2011a: Characteristics of precipitating convective systems in the South Asian monsoon. *J. Hydrometeorology*, **12**, 3-26, doi:10.1175/2010JHM1289.1.

Romatschke, U., and R. A. Houze, Jr., 2011b: Characteristics of precipitating convective systems in the premonsoon season of South Asia. *J. Hydrometeorology*, **12**, 157-180, doi:10.1175/2010JHM1311.1.

Romatschke, U., S. Medina, and R. A. Houze, Jr., 2010: Regional, seasonal, and diurnal variations of extreme convection in the South Asian region. *J. Climate*, **23**, 419-439, doi:10.1175/2009JCLI3140.1.

Rudlosky, S. D., and D. T. Shea, 2013: Evaluating WWLLN performance relative to TRMM/LIS. *Geophys. Res. Lett.*, **40**, 1-5, doi:10.1002/grl.50428.

Sato, T., 2013: Mechanism of orographic precipitation around the Meghalaya Plateau associated with intraseasonal oscillation and the diurnal cycle. *Mon. Wea. Rev.*, **141**, 2451-2466, doi:10.1175/MWR-D-12-00321.1.

Shukla, J., 1978: CISK-barotrophic-baroclinic instability and the growth of monsoon depressions. *J. Atmos. Sci.*, **35**, 495-508.

Shukla, R. P., 2014: The dominant intraseasonal mode of intraseasonal South Asian summer monsoon. *J. Geophys. Res.*, **119**, 635-651, doi:10.1002/2013JD020335.

Singh, S. V., and R. H. Kripalani, 1986: Application of extended empirical orthogonal function analysis to interrelationships and sequential evolution of monsoon fields. *Mon. Wea. Rev.*, **114**, 1603-1610.

Srinivasan, J., S. Gadgil, and P. J. Webster, 1993: Meridional propagation of large-scale monsoon convective zones. *Meteor. Atmos. Phys.*, **52**, 15-35.

Stephens, G. L., and Coauthors, 2002: The CloudSat mission and the A-train: A new dimension of space-based observations of clouds and precipitation. *Bull. Amer. Meteor. Soc.*, **83**, 1771-1790.

Vellore, R. K., R. Krishnan, J. Pendharkar, A. D. Choudhury, T. P. Sabin, 2014: On the anomalous precipitation enhancement over the Himalayan foothills during monsoon breaks. *Clim. Dyn.*, **43**, 2009-2031, doi:10.1007/s00382-013-2024-1.

Virts, K. S., and R. A. Houze, Jr., 2015a: Variation of lightning and convective rain fraction in mesoscale convective systems of the MJO. *J. Atmos. Sci.*, **72**, 1932-1944, doi:10.1175/JAS-D-14-0201.1.

Virts, K. S., and R. A. Houze, Jr., 2015b: Clouds and water vapor in the tropical tropopause transition layer over mesoscale convective systems. *J. Atmos. Sci.*, **72**, 4739-4753, doi:10.1175/JAS-D-15-0122.1.

Webster, P. J., and L. C. Chou, 1980: Low-frequency transitions of a simple monsoon system. *J. Atmos. Sci.*, **37**, 368-382.

Webster, P. J., L. Chou, and K. M. Lau, 1977: Mechanisms effecting the state, evolution and transition of the planetary scale monsoon. *Pageoph*, **115**, 1463-1492.

Webster, P. J., V. O. Magaña, T. N. Palmer, J. Shukla, R. A. Tomas, M. Yanai, and T. Yasunari, 1998: Monsoons: Processes, predictability, and the prospects for prediction. *J. Geophys. Res.*, **103**, 14451-14510.

Wilheit, T., C. D. Kummerow, and R. Ferraro, 2003: Rainfall algorithms for AMSR-E. *IEEE Trans. Geosci. Remote Sens.*, **41**, 204-214, doi:10.1109/TGRS.2002.808312.

Williams, M., and R. A. Houze, Jr., 1987: Satellite-observed characteristics of winter monsoon cloud clusters. *Mon. Wea. Rev.*, **115**, 505-519, doi:10.1175/1520-0493(1987)115<0505:SOCOWM>2.0.CO;2.

Yasunari, T., 1979: Cloudiness fluctuations associated with the Northern Hemisphere summer monsoon. *J. Meteor. Soc. Japan.*, **57**, 227-242.

Yasunari, T., 1980: A quasi-stationary appearance of 30 to 40 day period in the cloudiness fluctuations during the summer monsoon over India. *J. Meteor. Soc. Japan*, **58**, 225-229.

Yuan, J., and R. A. Houze, Jr., 2010: Global variability of mesoscale convective system anvil structure from A-Train satellite data. *J. Climate*, **23**, 5864-5888, doi:10.1175/2010JCLI3671.1.

Yuan, J., R. A. Houze, Jr., and A. J. Heymsfield, 2011: Vertical structures of anvil clouds of tropical messocale convective systems observed by CloudSat. *J. Atmos. Sci.*, **68**, 1653-1674, doi:10.1175/2011JAS3687.1.

Yuan, T., and X. Qie, 2008: Study on lightning and precipitation characteristics before and after the onset of the South China Sea summer monsoon. *J. Geophys. Res.*, **113**, D14101, doi:10.1029/2007JD009382.

Yuter, S. E., and R. A. Houze, Jr., 1998: The natural variability of precipitating clouds over the western Pacific warm pool. *Quart. J. Roy. Meteor. Soc.*, **124**, 53-99, doi:10.1002/qj.49712454504.

Zipser, E. J., 1994: Deep cumulonimbus cloud systems in the tropics with and without lightning. *Mon. Wea. Rev.*, **122**, 1837-1851.

Zipser, E. J., and K. R. Lutz, 1994: The vertical profile of radar reflectivity of convective cells: A strong indicator of storm intensity and lightning probability? *Mon. Wea. Rev.*, **122**, 1751-1759.

Zuidema, P., 2003: Convective clouds over the Bay of Bengal. *Mon. Wea. Rev.*, **131**, 780-798.

Table captions

Table 1. Methodology used by YH10 to identify cloud and precipitation features and MCSs, based on MODIS Tb_{11} and AMSR-E AE_Rain data. The cloud-top minimum temperature $Tb_{11RC1min}$ is defined as the mean Tb_{11} of the coldest decile of the largest raining core (RC1). Adapted from YHH11 and Virts and Houze (2015b).

Figure captions

Figure 1. Elevation (m), with 500-m contour in black. Blue polygons delineate three sub-regions: Meghalaya Plateau, northeast Himalayan notch, and Bay of Bengal.

Figure 2. Seasonal-mean (top-bottom) ERA-Interim 925-hPa winds (vectors) and geopotential height (contours; m), TRMM precipitation (mm day^{-1}), and WWLLN lightning frequency (strokes km^{-2} $year^{-1}$), averaged over (left-right) pre-monsoon [April-May (AM)], monsoon [June-September (JJAS)], and post-monsoon months [October-November (ON)]. Black contours indicate the 500-m elevation.

Figure 3. Seasonal-mean density of (top-bottom) small SMCSs, large SMCSs, and CMCSs during (left-right) AM, JJAS, and ON, expressed as number of systems per $0.5° \times 0.5°$ grid box per month (note that the color scales differ). Black contours indicate the 500-m elevation.

Figure 4. CFADs of CloudSat reflectivities in the precipitating portions of (top-bottom) small SMCSs, large SMCSs, and CMCSs over the Bay of Bengal during (a-c) AM, JJAS, and ON. Each CFAD is normalized such that its maximum value is 1. (d) Difference between CFADs for JJAS and AM, with blue shading indicating where reflectivity values are proportionately more likely to be observed during AM. Sample size is indicated in upper right corner of each panel.

Figure 5. As in 4, but for the anvil portions of large SMCSs and CMCSs.

Figure 6. WWLLN lightning counts (strokes hr^{-1}) within the radius of the high-cloud shields of (a) small SMCSs, (b) large SMCSs, and (c) CMCSs over the Bay of Bengal as a function of season. Error bars represent the 95% confidence interval. Note that the ordinate scales vary by MCS type.

Figure 7. CFADs of CloudSat reflectivities in the (top) precipitating and (bottom) anvil portions of MCSs over the Meghalaya Plateau during (a) AM and (b) JJAS. (c) Difference between CFADs for JJAS and AM. Sample size is indicated in upper right corner of panels in the top row.

Figure 8. CFADs of CloudSat reflectivities in the (top) precipitating and (bottom) anvil portions of MCSs over the northeast Himalayan notch during JJAS. Sample size is indicated in the upper right corner of the top panel.

Figure 9. Anomalies of ERA-Interim 925-hPa wind (vectors) and geopotential height (contours; CI=2 m) for days when a (a) large SMCS or (b) CMCS was observed over the Bay of Bengal (black outlined region) during JJAS. Black contours indicate the 500-m elevation.

Figure 10. Anomalies of ERA-Interim 850-hPa wind (vectors) and geopotential height (contours; CI=2 m) for days when an MCS was observed over the Meghalaya Plateau (black outlined region) during JJAS. Black contours indicate the 500-m elevation.

Figure 11. (a) Anomalies of ERA-Interim 850-hPa wind (vectors) and geopotential height (contours; CI=2 m) for days when an MCS was observed over the northeast Himalayan notch

(black outlined region) during JJAS. (b) As in (a), but CI=0.4 m. (c) As in (a), but for CAPE anomalies. Black contours indicate the 500-m elevation.

Figure 12. Anomalies of ERA-Interim 925-hPa wind (vectors) and geopotential height (contours; CI=2 m) during eight BSISO1 phases during JJAS. Black contours indicate the 500-m elevation.

Figure 13. Active minus break (a) TRMM precipitation (mm day^{-1}) and (b) WWLLN lightning (strokes km^{-2} $year^{-1}$), based on BSISO1 index during JJAS. Black contours indicate the 500-m elevation.

Figure 14. Density of (top-bottom) small SMCSs, large SMCSs, and CMCSs, expressed as number of systems per $0.5° \times 0.5°$ grid box (note that the color scales differ) for (a) active and (b) break BSISO1 periods during JJAS and (c) the difference between them. Black contours indicate the 500-m elevation.

Figure 15. Number of MCSs observed over each region during each BSISO1 phase during JJAS.

Figure 16. CFADs of CloudSat reflectivities in the precipitating portions of (top) large SMCSs and (bottom) CMCSs over the Bay of Bengal during locally (a) rainy and (b) dry BSISO1 periods during JJAS. (c) Difference between locally rainy and dry CFADs, with blue shading indicating where reflectivity values are proportionately more likely to be observed during the dry period. Sample size is indicated in upper right corner of each panel.

Figure 17. As in Fig. 16, but for CloudSat profiles sampling the anvil portions of MCSs.

Figure 18. Regional-mean TRMM precipitation (gray lines; scale at right; mm day^{-1}) and WWLLN lightning counts (black lines; scale at left; strokes hr^{-1}) within the radius of the high-cloud shields of MCSs over (a) the Meghalaya Plateau and (b) the Bay of Bengal as a function of BSISO1 phase during JJAS. Error bars represent the 95% confidence interval. Note that the ordinate scales vary by region.

Figure 19. CFADs of CloudSat reflectivities in (top) precipitating and (bottom) anvil portions of MCSs over the Meghalaya Plateau during the locally (a) rainy and (b) dry BSISO1 periods during JJAS. (c) Difference between locally rainy and dry CFADs. Sample size is indicated in upper right corner of each panel in the top row.

Table 1. Methodology used by YH10 to identify cloud and precipitation features and MCSs, based on MODIS Tb_{11} and AMSR-E AE_Rain data. The cloud-top minimum temperature $Tb_{11RC1min}$ is defined as the mean Tb_{11} of the coldest decile of the largest raining core (RC1). Adapted from YHH11 and Virts and Houze (2015b).

Abbreviation	Name	Definition
HCC	High cloud complex	Region of MODIS Tb_{11} contained within a single 260 K isotherm
HCS	High cloud system	Portion of HCC associated with a particular minimum value of Tb_{11}
PF	Precipitation feature	Region of AMSR-E AE_Rain parameter surrounded by 1 mm h^{-1} contour
RC	Raining core	Portion of any PF overlapping and/or located within an HCS
HRA	Heavy rain area	Portion of PF with rain rate greater than 6 mm h^{-1}
MCS	Mesoscale convective system	Any HCS whose largest RC satisfies the following criteria: 1) Exceeds 2000 km^2 in total area 2) Accounts for more than 70% of the total area with rain rate greater than 1 mm h^{-1} inside the HCS 3) Minimum cloud-top temperature above the RC (indicated by $Tb_{11RC1min}$) is less than 220 K 4) More than 10% of RC is occupied by HRAs
SMCS	Separated MCS	The largest RC of the MCS is part of a PF that contains less than three dominant RCs of any MCS
CMCS	Connected MCS	The largest RC of the MCS is part of a PF that contains dominant RCs of at least three MCSs

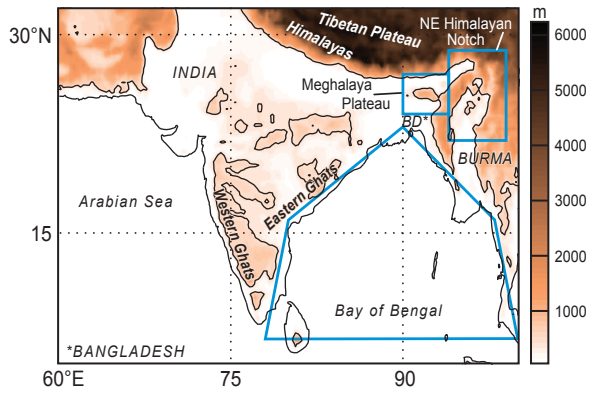

Figure 1. Elevation (m), with 500-m contour in black. Blue polygons delineate three sub-regions: Meghalaya Plateau, northeast Himalayan notch, and Bay of Bengal.

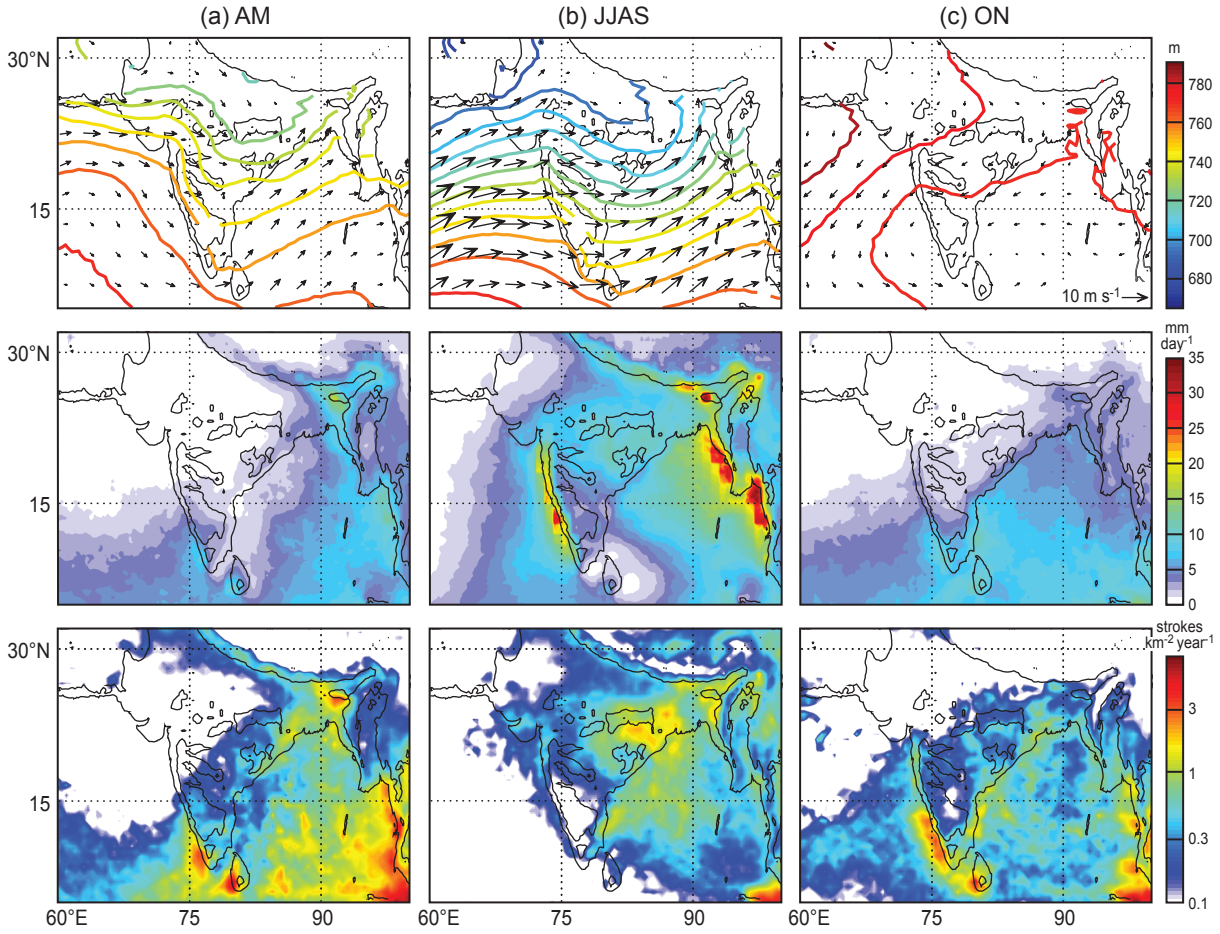

Figure 2. Seasonal-mean (top-bottom) ERA-Interim 925-hPa winds (vectors) and geopotential height (contours; m), TRMM precipitation (mm day^{-1}), and WWLLN lightning frequency (strokes km^{-2} year^{-1}), averaged over (left-right) pre-monsoon [April-May (AM)], monsoon [June-September (JJAS)], and post-monsoon months [October-November (ON)]. Black contours indicate the 500-m elevation.

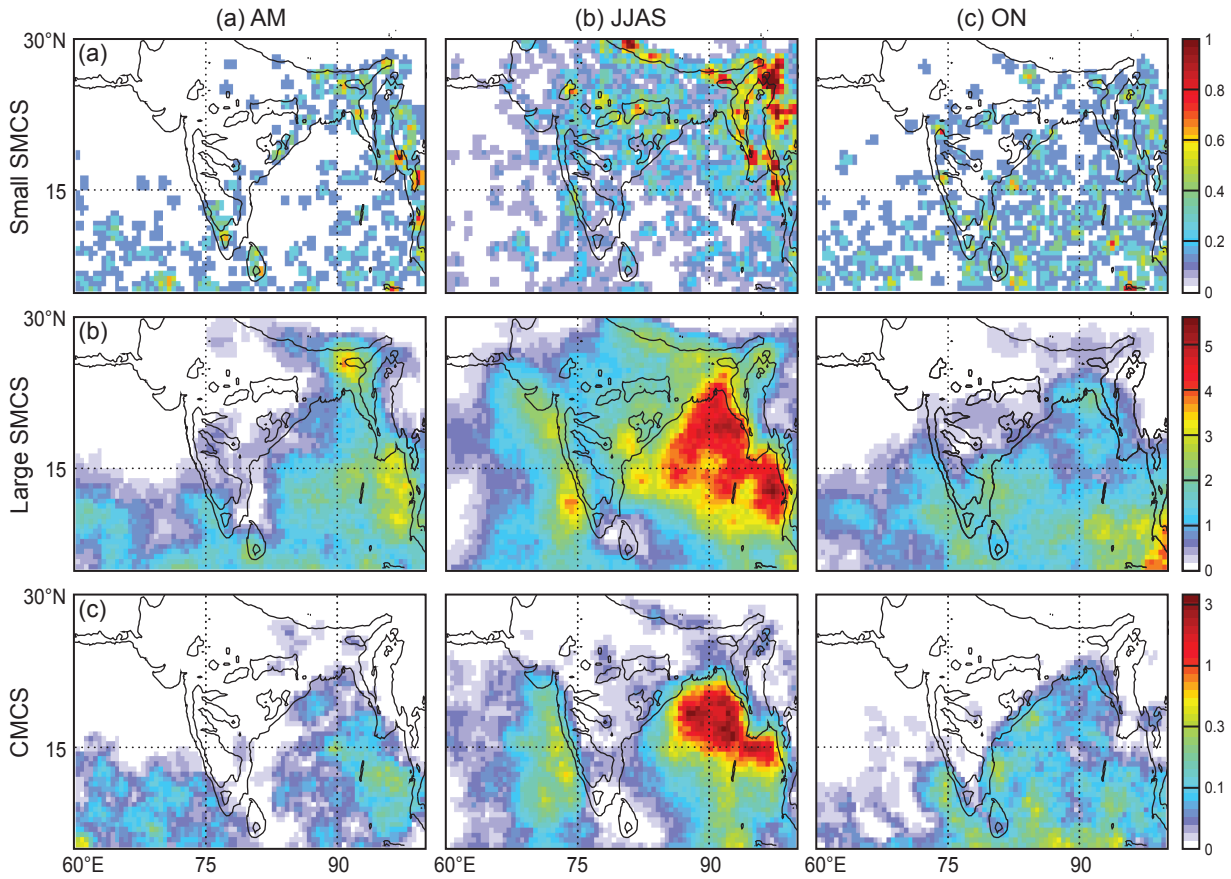

Figure 3. Seasonal-mean density of (top-bottom) small SMCSs, large SMCSs, and CMCSs during (left-right) AM, JJAS, and ON, expressed as number of systems per 0.5° × 0.5° grid box per month (note that the color scales differ). Black contours indicate the 500-m elevation.

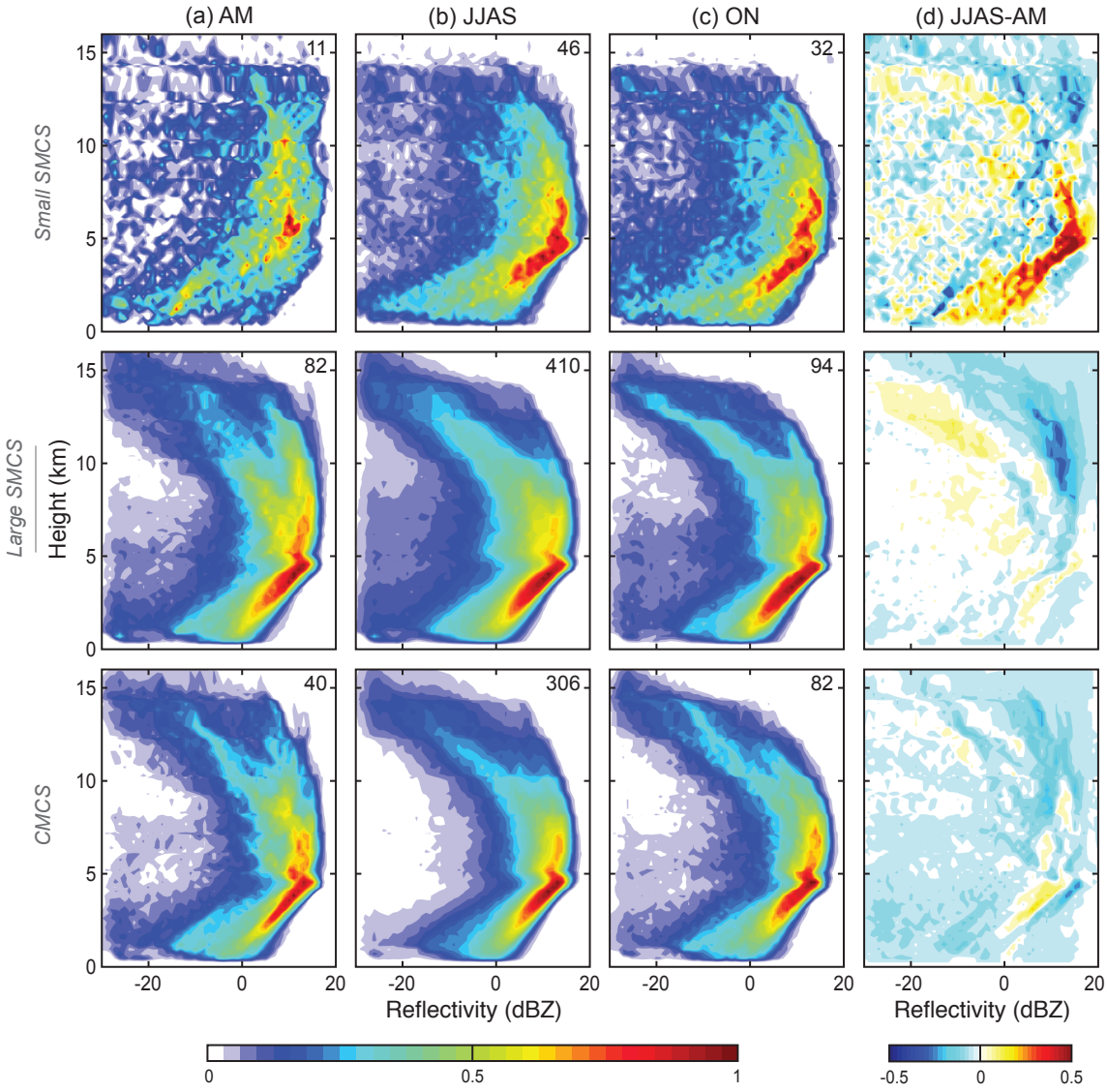

Figure 4. CFADs of CloudSat reflectivities in the precipitating portions of (top-bottom) small SMCSs, large SMCSs, and CMCSs over the Bay of Bengal during (a-c) AM, JJAS, and ON. Each CFAD is normalized such that its maximum value is 1. (d) Difference between CFADs for JJAS and AM, with blue shading indicating where reflectivity values are proportionately more likely to be observed during AM. Sample size is indicated in upper right corner of each panel.

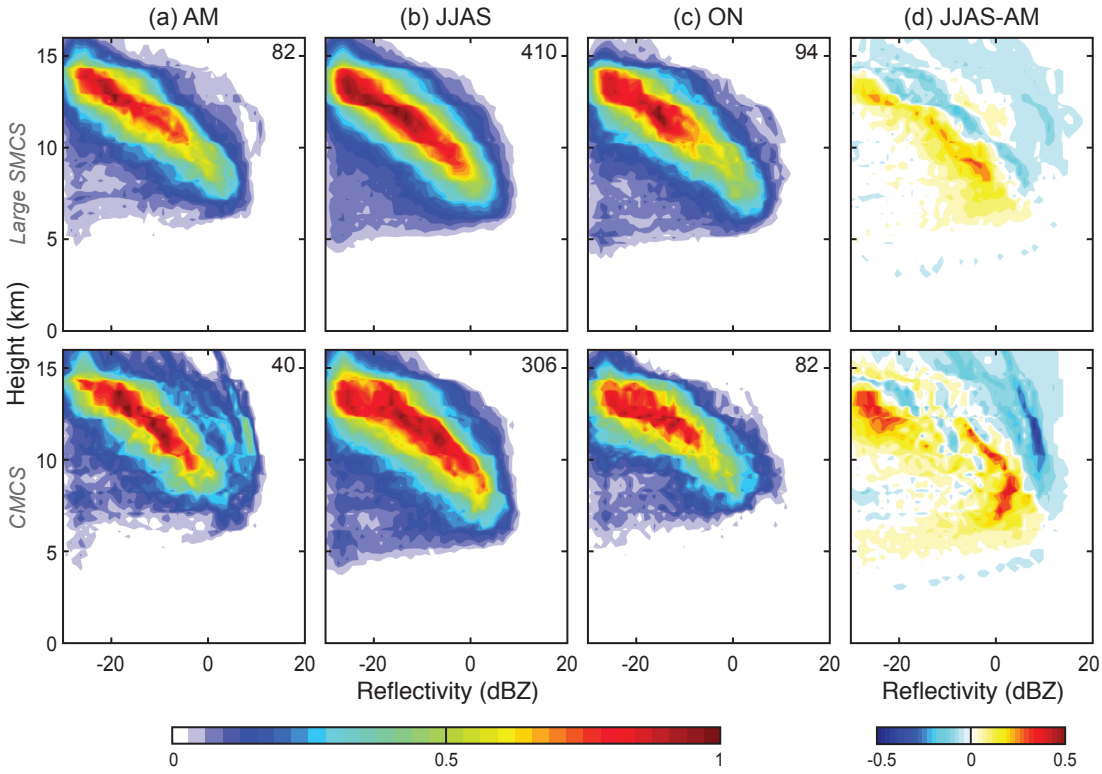

Figure 5. As in 4, but for the anvil portions of large SMCSs and CMCSs.

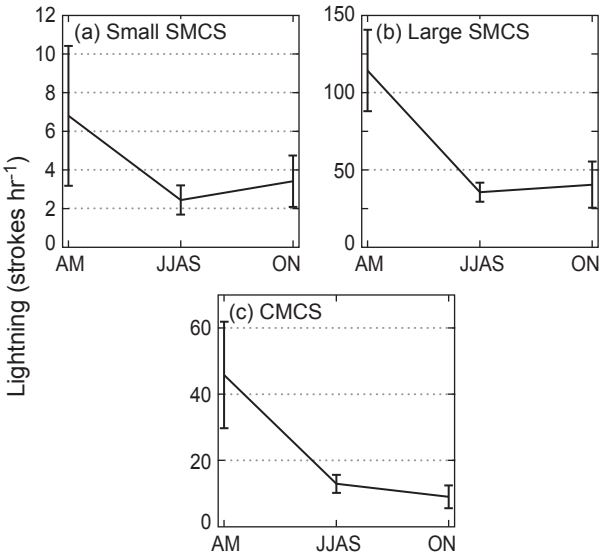

Figure 6. WWLLN lightning counts (strokes hr^{-1}) within the radius of the high-cloud shields of (a) small SMCSs, (b) large SMCSs, and (c) CMCSs over the Bay of Bengal as a function of season. Error bars represent the 95% confidence interval. Note that the ordinate scales vary by MCS type.

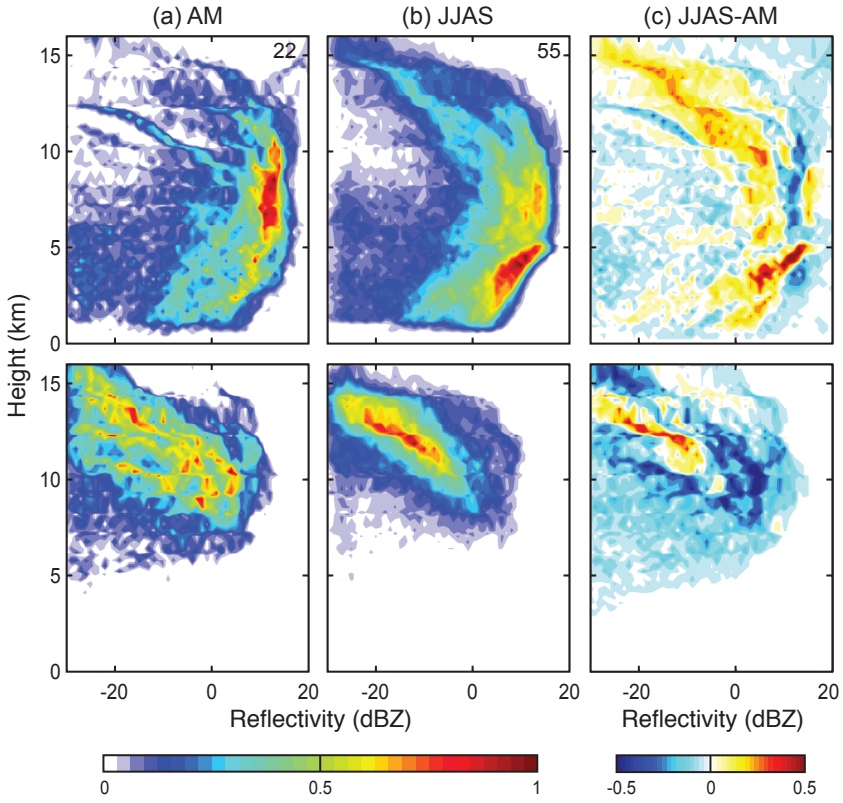

Figure 7. CFADs of CloudSat reflectivities in the (top) precipitating and (bottom) anvil portions of MCSs over the Meghalaya Plateau during (a) AM and (b) JJAS. (c) Difference between CFADs for JJAS and AM. Sample size is indicated in upper right corner of panels in the top row.

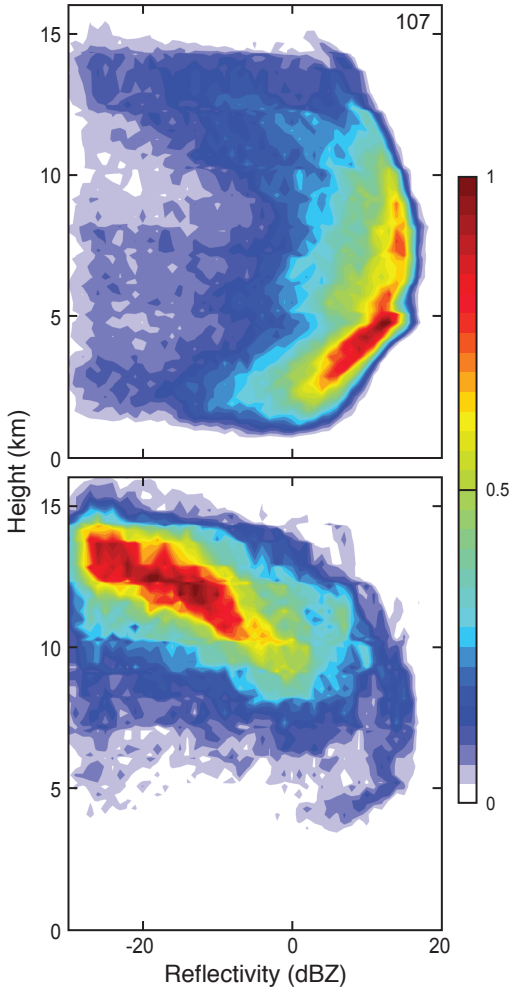

Figure 8. CFADs of CloudSat reflectivities in the (top) precipitating and (bottom) anvil portions of MCSs over the northeast Himalayan notch during JJAS. Sample size is indicated in the upper right corner of the top panel.

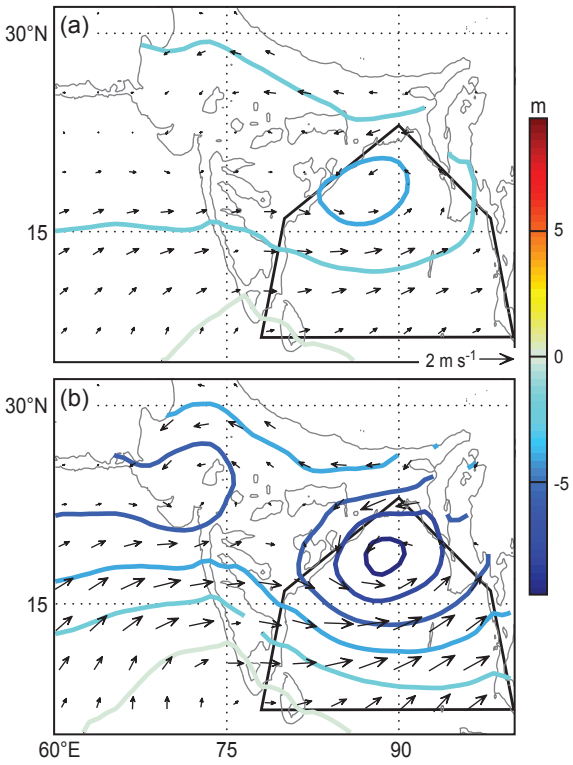

Figure 9. Anomalies of ERA-Interim 925-hPa wind (vectors) and geopotential height (contours; CI=2 m) for days when a (a) large SMCS or (b) CMCS was observed over the Bay of Bengal (black outlined region) during JJAS. Black contours indicate the 500-m elevation.

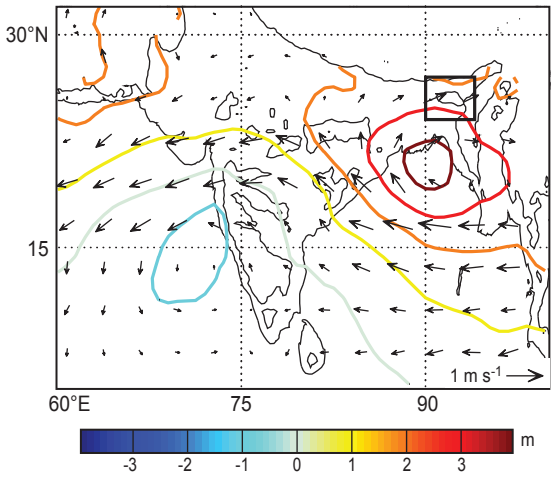

Figure 10. Anomalies of ERA-Interim 850-hPa wind (vectors) and geopotential height (contours; CI=2 m) for days when an MCS was observed over the Meghalaya Plateau (black outlined region) during JJAS. Black contours indicate the 500-m elevation.

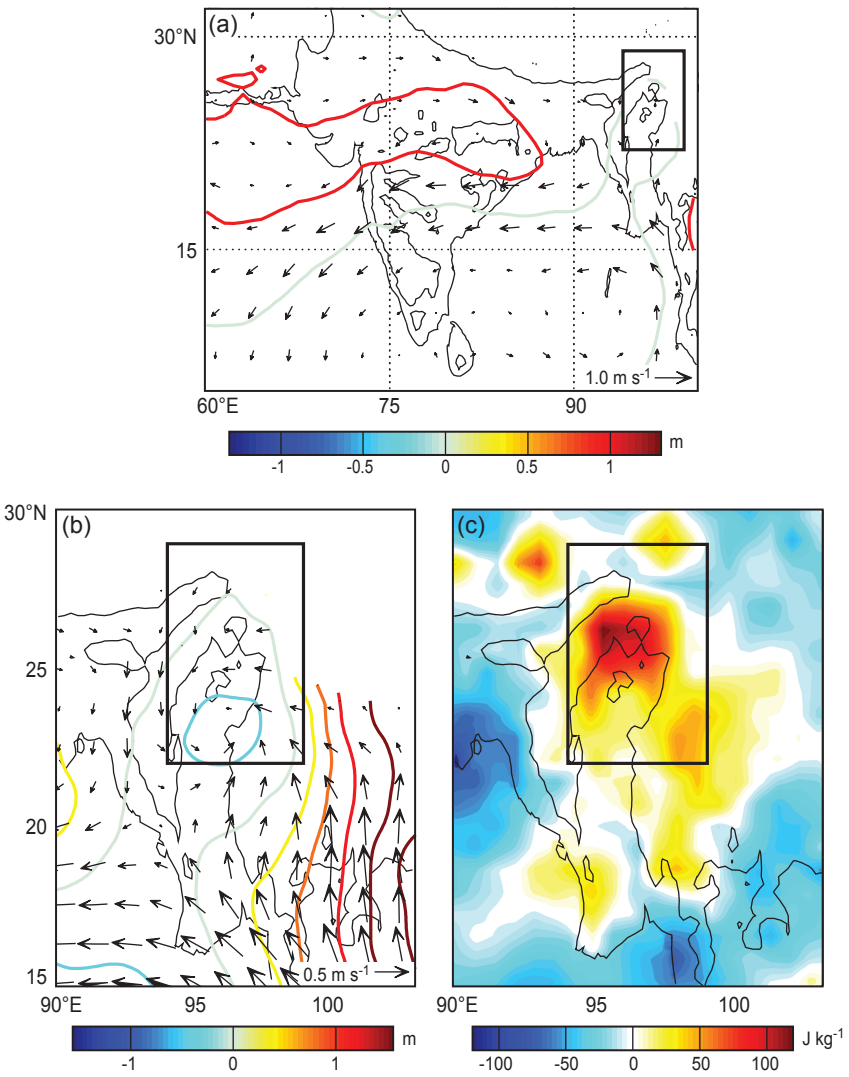

Figure 11. (a) Anomalies of ERA-Interim 850-hPa wind (vectors) and geopotential height (contours; CI=2 m) for days when an MCS was observed over the northeast Himalayan notch (black outlined region) during JJAS. (b) As in (a), but CI=0.4 m. (c) As in (a), but for CAPE anomalies. Black contours indicate the 500-m elevation.

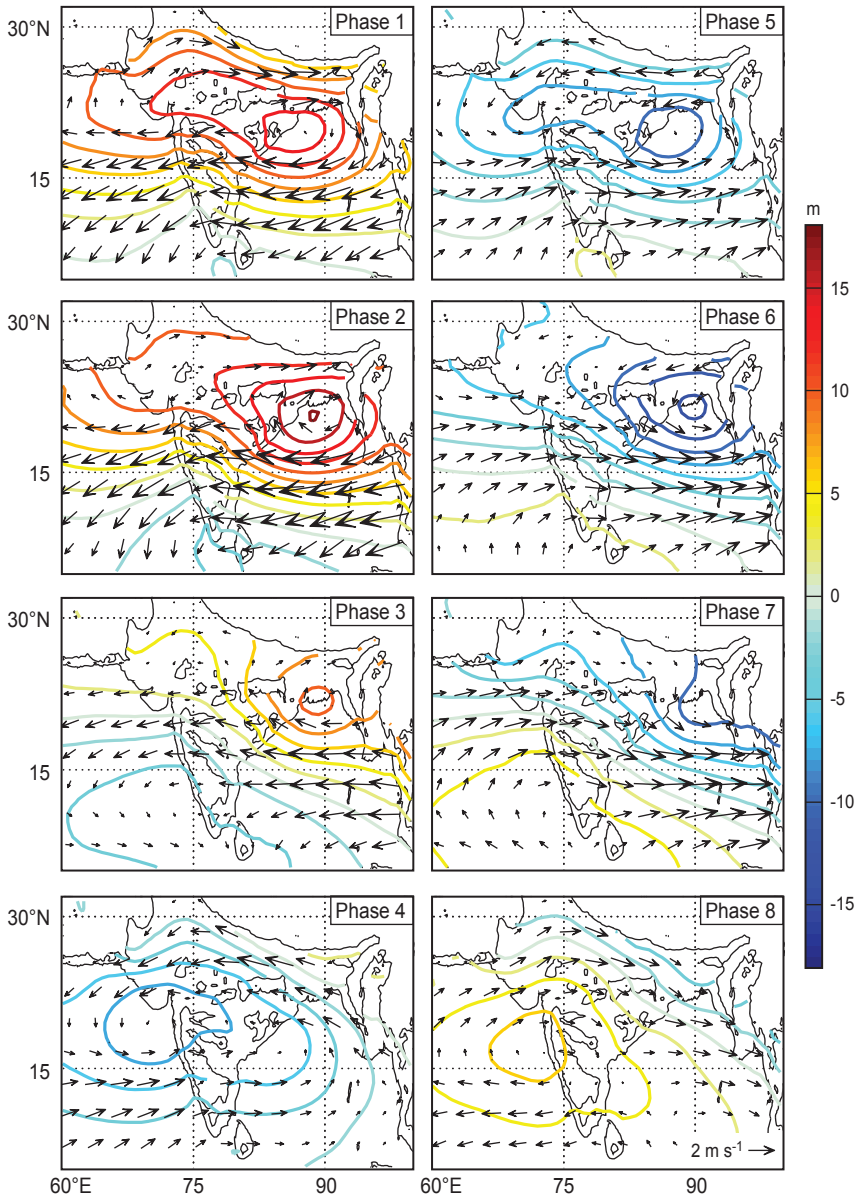

Figure 12. Anomalies of ERA-Interim 925-hPa wind (vectors) and geopotential height (contours; CI=2 m) during eight BSISO1 phases during JJAS. Black contours indicate the 500-m elevation.

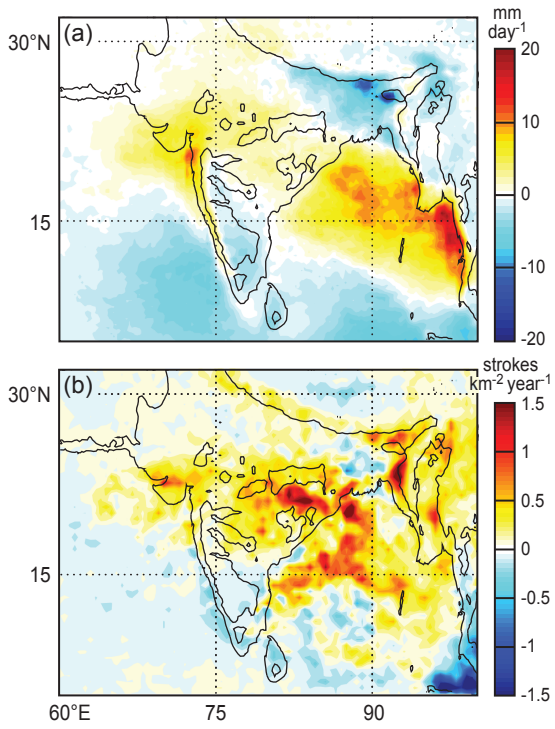

Figure 13. Active minus break (a) TRMM precipitation (mm day^{-1}) and (b) WWLLN lightning (strokes km^{-2} year^{-1}), based on BSISO1 index during JJAS. Black contours indicate the 500-m elevation.

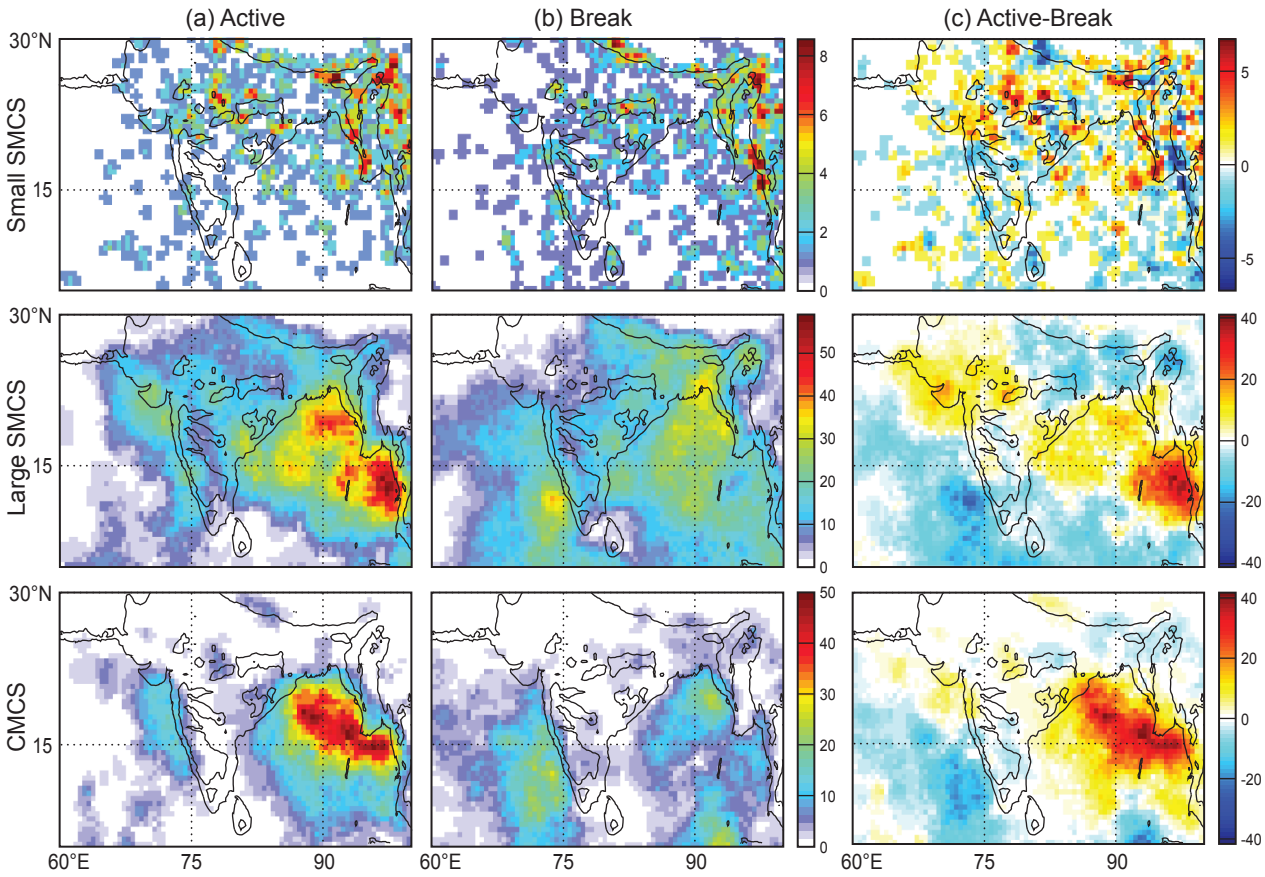

Figure 14. Density of (top-bottom) small SMCSs, large SMCSs, and CMCSs, expressed as number of systems per 0.5° × 0.5° grid box (note that the color scales differ) for (a) active and (b) break BSISO1 periods during JJAS and (c) the difference between them. Black contours indicate the 500-m elevation.

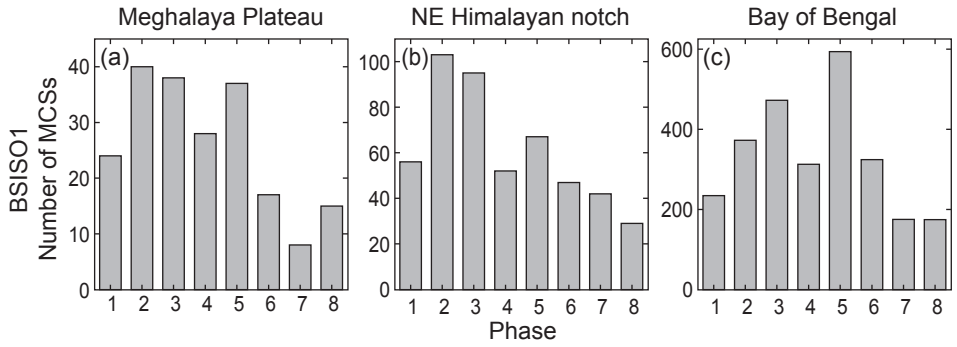

Figure 15. Number of MCSs observed over each region during each BSISO1 phase during JJAS.

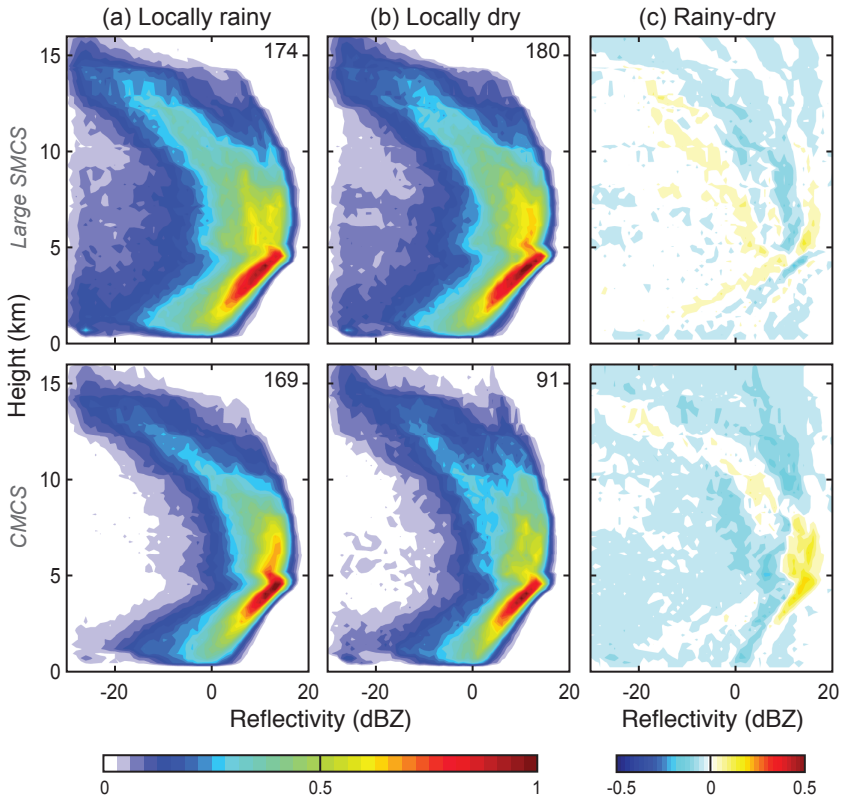

Figure 16. CFADs of CloudSat reflectivities in the precipitating portions of (top) large SMCSs and (bottom) CMCSs over the Bay of Bengal during locally (a) rainy and (b) dry BSISO1 periods during JJAS. (c) Difference between locally rainy and dry CFADs, with blue shading indicating where reflectivity values are proportionately more likely to be observed during the dry period. Sample size is indicated in upper right corner of each panel.

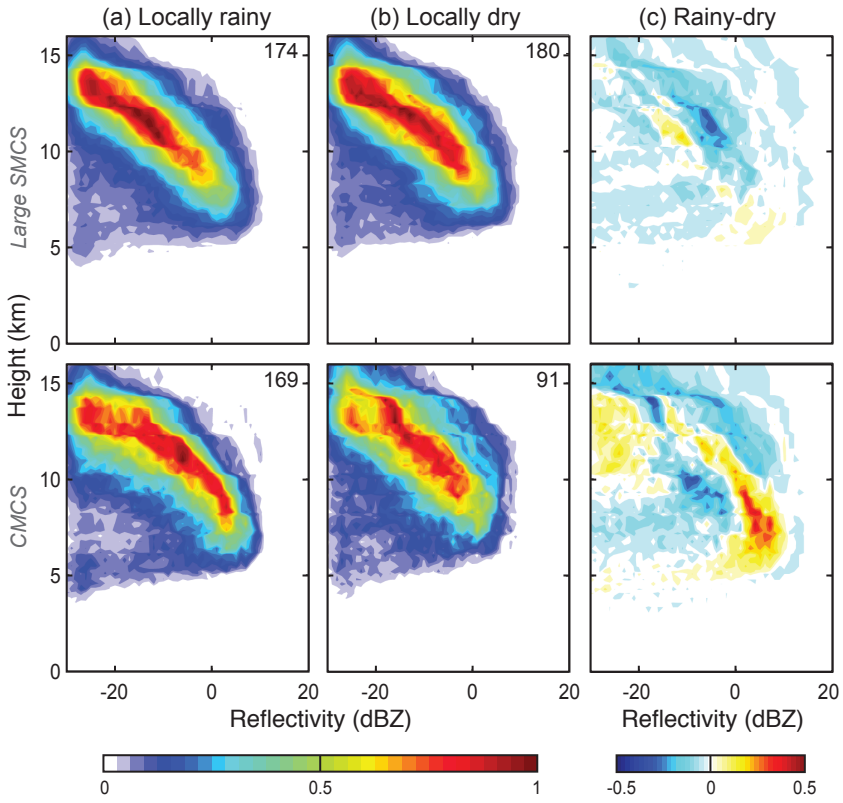

Figure 17. As in Fig. 16, but for CloudSat profiles sampling the anvil portions of MCSs.

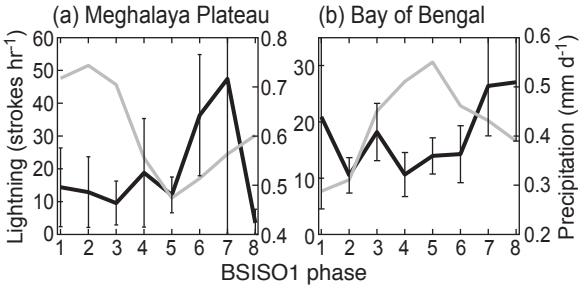

Figure 18. Regional-mean TRMM precipitation (gray lines; scale at right; mm day^{-1}) and WWLLN lightning counts (black lines; scale at left; strokes hr^{-1}) within the radius of the high-cloud shields of MCSs over (a) the Meghalaya Plateau and (b) the Bay of Bengal as a function of BSISO1 phase during JJAS. Error bars represent the 95% confidence interval. Note that the ordinate scales vary by region.

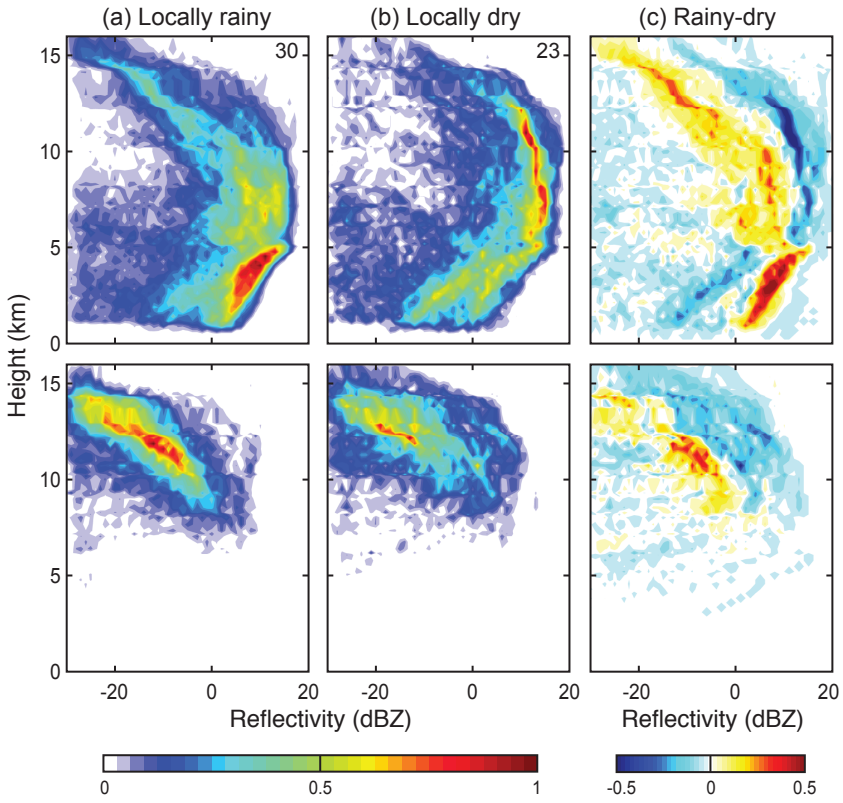

Figure 19. CFADs of CloudSat reflectivities in (top) precipitating and (bottom) anvil portions of MCSs over the Meghalaya Plateau during the locally (a) rainy and (b) dry BSISO1 periods during JJAS. (c) Difference between locally rainy and dry CFADs. Sample size is indicated in upper right corner of each panel in the top row.